

LS Scienza dei Materiali - a.a. 2005/06

## Fisica delle Nanotecnologie – part 9

Version 4, Dec 2005

Francesco Fuso, tel 0502214305, 0502214293 - fuso@df.unipi.it

<http://www.df.unipi.it/~fuso/dida>

# **Tecnologie convenzionali nell'approccio top-down; II: metodi e problematiche di litografia ottica ed elettronica ed alternative emergenti**

14/12/2005 – 16.30-18 – room O

# Introduction to the topic I

Within the term **lithography** we include all processes needed to define a (lateral) pattern onto a substrate (or a multilayered structure)

In an oversimplified picture:

We use an **(material or immaterial)** “ink” to define a pattern;

We can either define a complex pattern all at once (**parallel process**), or draw it “pixel by pixel” (**serial, or scanning, process**);

The ink is used to modify *locally* the substrate surface (**impression**);

If required, the substrate can be previously prepared so to be sensitive to the ink (**photoresist or resist-assisted** lithography)

An **etching** process is used to locally remove the material (either in impressed or non impressed regions, i.e., **subtractive or additive** lithography), thus to transfer the defined pattern to the substrate

Note: sometimes, instead of etching direct deposition of ink can be used (*as we will see, e.g., in atom lithography*)

Thus, lithography comprises of several aspects, including, e.g.,:

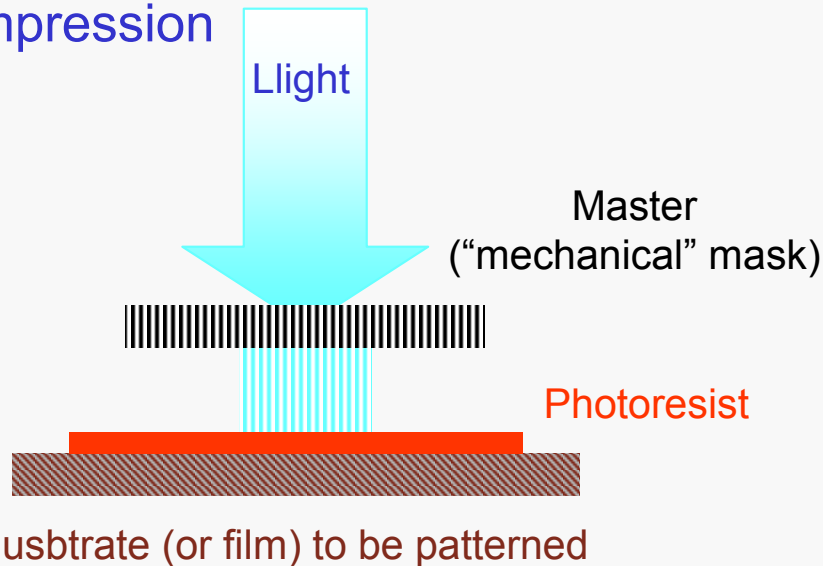
- Methods to create a patterned ink;
- Techniques for impression;
- Etching processes

# Introduction to the topic II

**Optical lithography** is the most common (and most simple) method in microelectronics

## Simplified picture of a subtractive process

### 1. Impression



### 2. Development



### 3. Etching



## Essential components:

Light (to make impression)

Mask (to produce the pattern)

Photoresist (to be impressed)

Development and etching (to transfer the pattern)

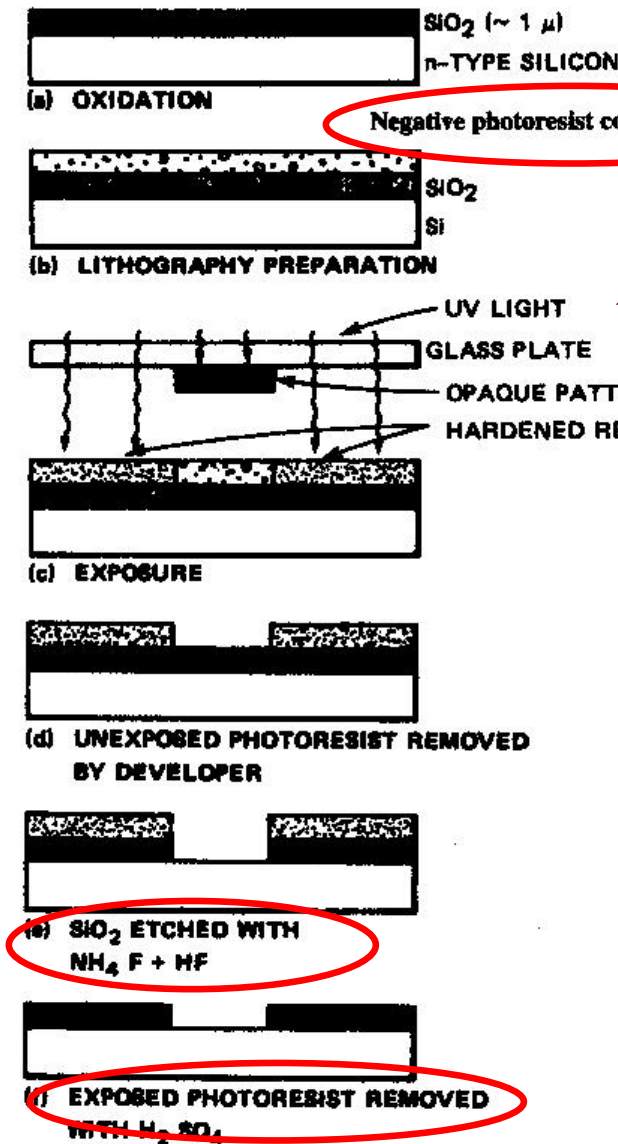
## Inherent advantages:

- **parallel operation (large-scale impressions in a single run)**
- **flexibility/suitability for large scale integration**

# Outlook

1. Optical lithography as the most common technique in microelectronics
  - A. Basic processes;
  - B. Photoresists and masks
2. Optical microscopy and the role of diffraction in lithography
3. Strategies to improve space resolution
4. Electron microscopy and related issues
5. Lithographies with charged particle beams
6. Lithographies and direct deposition with neutral atoms
7. A very few words on nanoimprints

# 1.A. Basic processes in optical lithography



Complex sequence of steps (even in very basic processes)

Negative and positive resists exist

Space definition *always* affected by "geometrical" issues

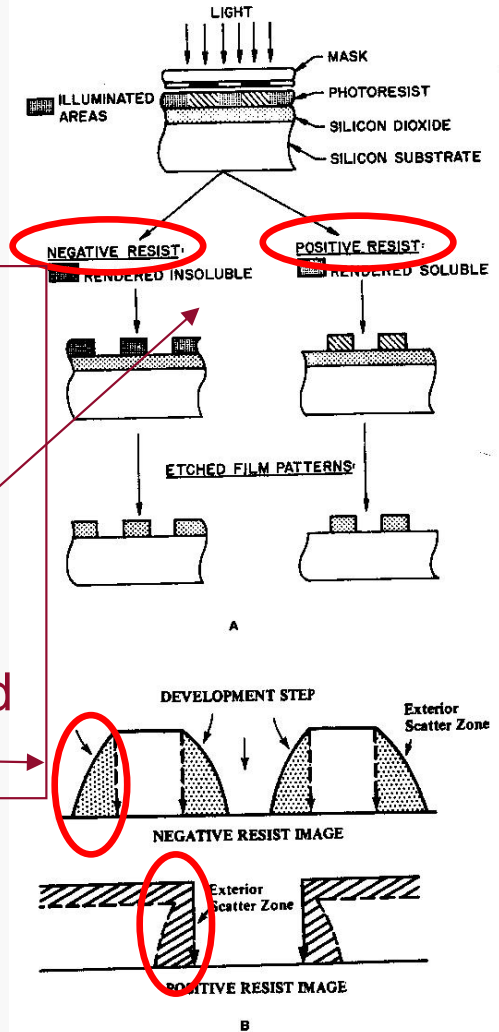


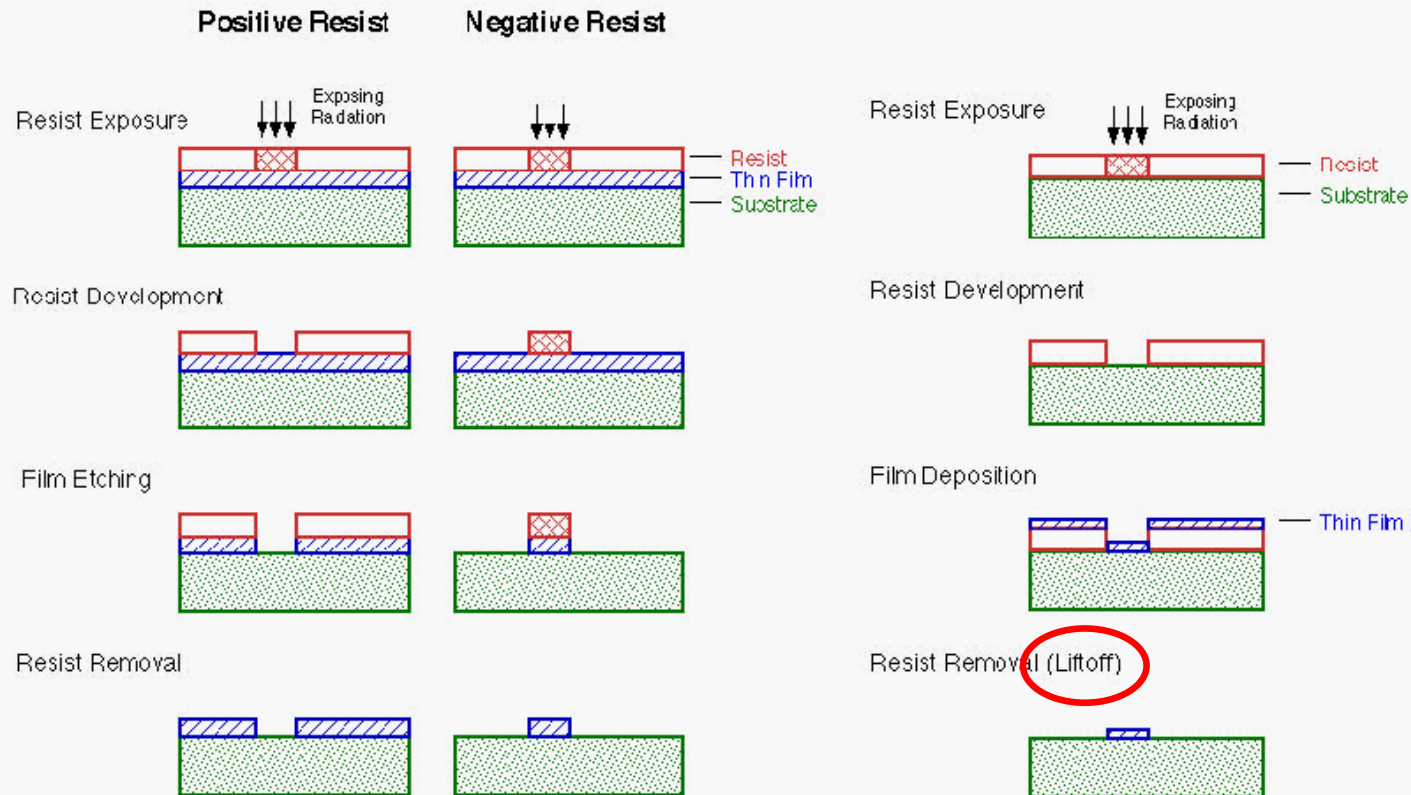
Figure 1.1 Positive and negative resist exposure, development, and edge-scattered radiation. (A) Positive and negative resists, exposure, and development. Positive resists develop in the exposed region and usually remain soluble for lift-off. Negative resists remain in the exposed region but are insoluble and not suitable for lift-off (see text). (B) Edge-scattered radiation profile for negative and positive resists. Time-independent development of cross-linked negative resist fails to remove light scatter zone. Development of positive resist rapidly removes exposed region and can be quenched to inhibit removal of lateral scattered exposed resist region. (From Brodie, I. and J. J. Murray, The Physics of Microfabrication, Plenum Press, New York, 1982. With permission.)

Figure 1.22 Basic IC process steps on an oxidized Si wafer; photolithography (with a negative-tone resist), including exposure, development, oxide etching, and resist stripping. (From Brodie, I. and J. J. Murray, The Physics of Microfabrication, Plenum Press, New York, 1991. With permission.)

Da M. Madou, Fundamentals of microfab., CRC (1997)

# Example of process flexibility in lithography

Two type of **pattern transfer**(subtractive or additive)



Subtraction or addition of features feasible (through combination with other techniques, e.g., deposition, liftoff,...)

# 1.B. Photoresists

## Contrast curve for ideal photoresists

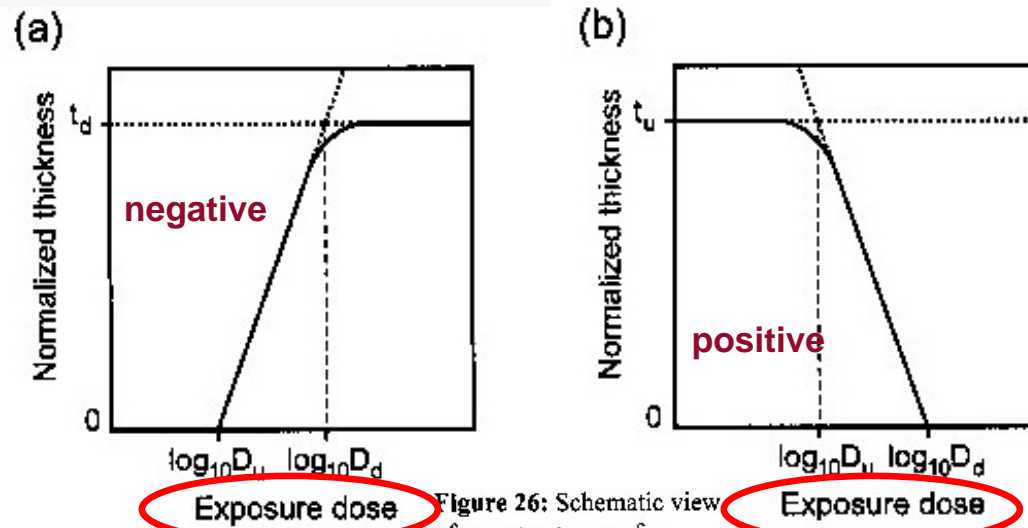


Figure 26: Schematic view of a contrast curve for (a) negative tone resist and (b) positive tone resist.

### Essential requirements:

- high sticking coefficient;
- homogeneity;
- uniform thickness;
- high sensitivity to radiation (typ. UV);
- fidelity in pattern reproduction

### “Sensitivity”:

$N = \text{number of broken bonds} = G \cdot \text{dose} / 100$   
With dose expressed in eV:  $G_{\text{typ}} \sim 1-10$

### Typical choices for photoresist:

- ✓ Light-sensitive polymers (or organic amorphous materials)
- ✓ UV-broken bonds modify features (protect/unprotect against etching)
- ✓ Thickness kept below the micrometer level to improve homogeneity and reduce dose (and enhance space resolution)

# 7 Photoresist

Photoresists are also an integral part of lithography. The performance of the resist is the determining factor for the magnitude of the technology factor  $k_1$ . In general, photoresists are polymers which react when exposed to light. There are two different types of resists: With positive tone resists, the exposed areas of the resist will dissolve in the developer, with negative tone resists, the exposed areas will remain.

Positive tone resists consist of three components, a resin, which serves as a binder and establishes the mechanical properties, a photoactive compound (PAC), and a solvent to keep the resist liquid. The resin is not normally responsive to the exposure. The commonly used positive tone resist system for g- and i-line lithography is the novolac/diazonaphthoquinones (DNQ) system. The novolac is the resin material and dissolves in aqueous bases. The DNQ is the PAC, but when unexposed it acts as a dissolution inhibitor. Figure 22 shows the reaction cycle of the DNQ upon exposure. Upon exposure  $N_2$  is split off the molecule. After a rearrangement, the molecule undergoes a reaction with the  $H_2O$ , which stems from the air. The reaction product now does not behave as a dissolution inhibitor, but as a dissolution enhancer. Therefore the exposed areas of the resist will dissolve about 100 times quicker than the unexposed areas.

Negative tone resists also consist of the three compounds: resin, photoactive compound and a solvent to keep the resist liquid. The resin consists of a cyclic synthetic rubber, which is not radiation-sensitive, but strongly soluble in the developer (non-polar organic solvents). The PAC is normally a bis-arylazide. Figure 23 shows the chemical structure of a rubber resin and a PAC. Upon exposure, the PAC dissociates into nitrene and  $N_2$ . These nitrene molecules are able to react with the rubber molecules, so a cross-linking between two rubber molecules can be established. Thus a three-dimensional cross-linked molecular network is formed, which is insoluble in the developer.

As device dimensions are scaled down further, the g-line steppers as well as the novolac/DNQ resists have been improved, so the features for 350 nm generation could be printed. But reaching the 250 nm generation, the illumination wavelength was shifted to 250 nm, too. However, at this wavelength novolac and DNQ do strongly absorb the light, therefore another class of resists had to be developed. Furthermore, the intensity of

# A few examples of photoresists

## Positive resist

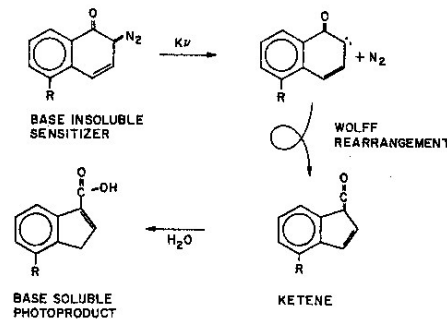


Figure 22: Exposure process of positive tone DNQ-resists [38], [39].

## Negative resist

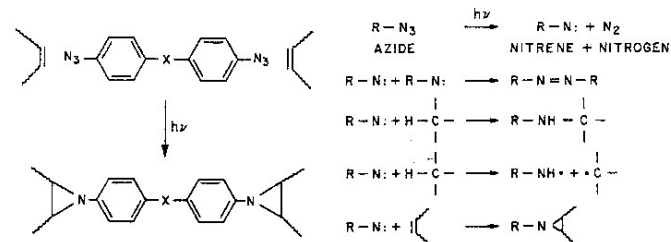


Figure 23: Reaction cycle of a negative tone resist during exposure [38], [39].

Da R. Waser Ed., Nanoelectronics and information technology (Wiley-VCH, 2003)

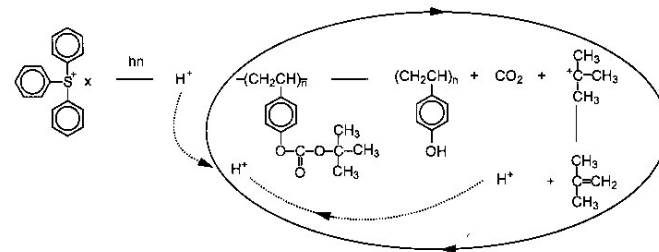
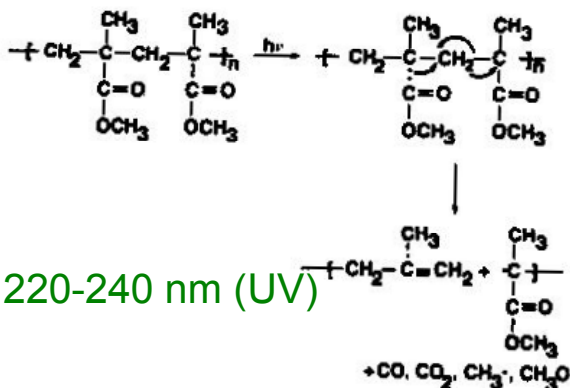


Figure 24: Chemical amplification cycle in a CAR [40].

## Poly(methylmethacrylate) or PMMA

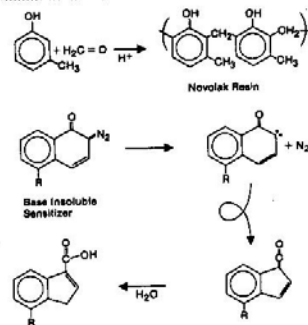
Photo-induced chain scission of PMMA resist.



$\lambda = 220-240 \text{ nm (UV)}$

## Diazoquinone ester (DQ) and phenolic novolak resin (N), i.e., DQN

The novolak (Novolak) matrix resin (N) is prepared by acid copolymerization of cresol and formaldehyde. The base insoluble sensitizer, a diazoquinone (DQ), undergoes photolysis to produce a carbene which then undergoes a rearrangement to form a ketene. The ketene reacting with water present in the film forms a base-soluble, indenecarboxylic acid photoproduct.



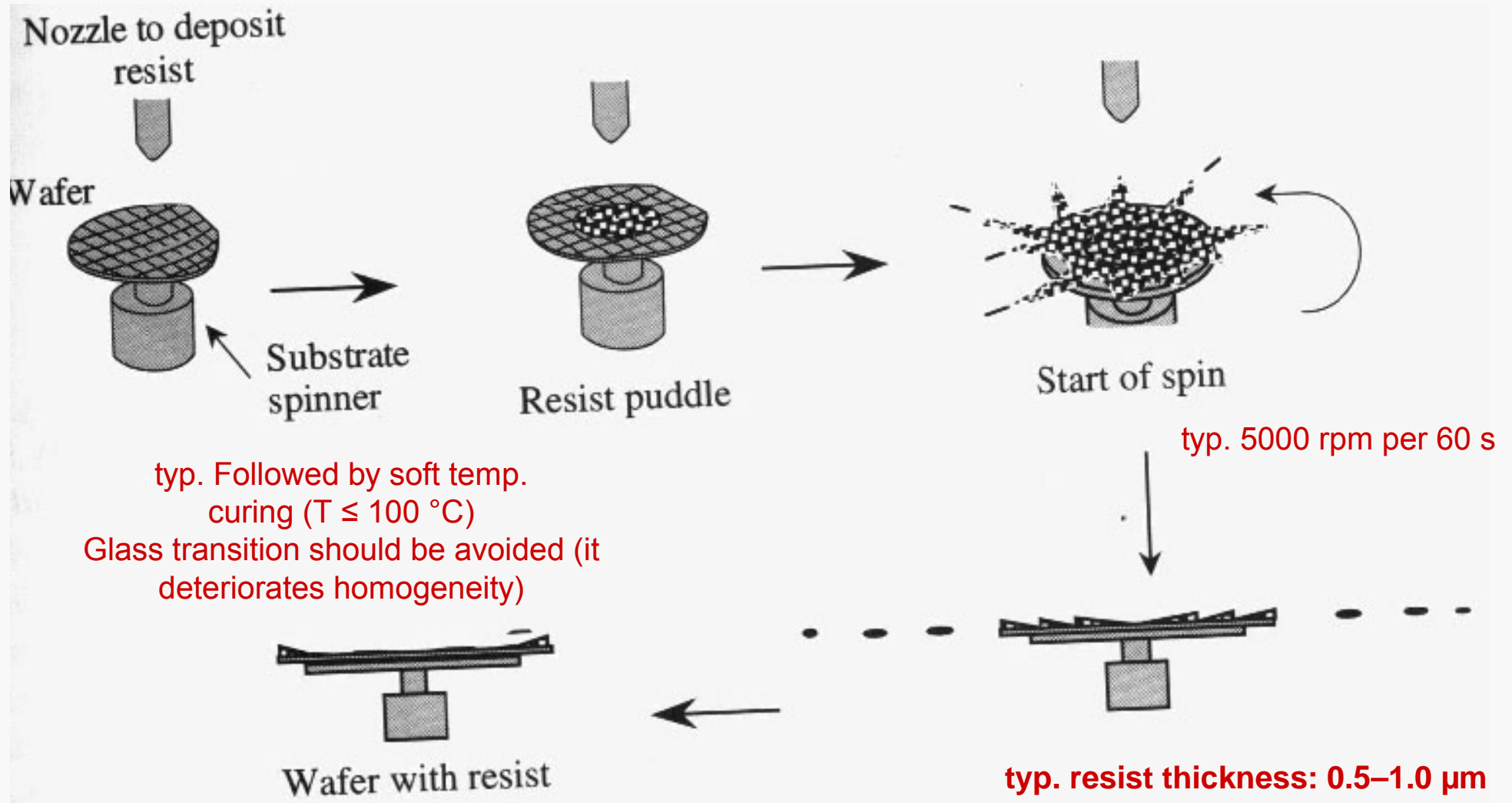
## Positive resists

$\lambda = 365 \text{ nm (Hg-lamps)}$

Well established photochemistry features

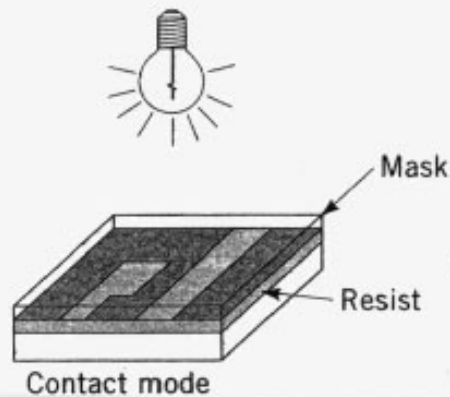
# Deposition of photoresists

Most frequently used system: **spin-coating** (simple, scalable, effective, cheap,...)

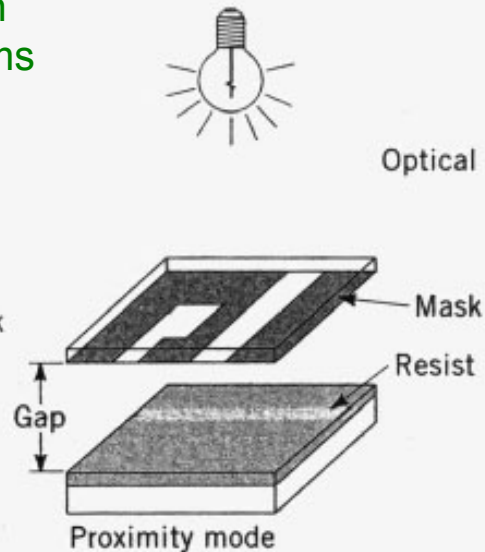


# Mask configurations

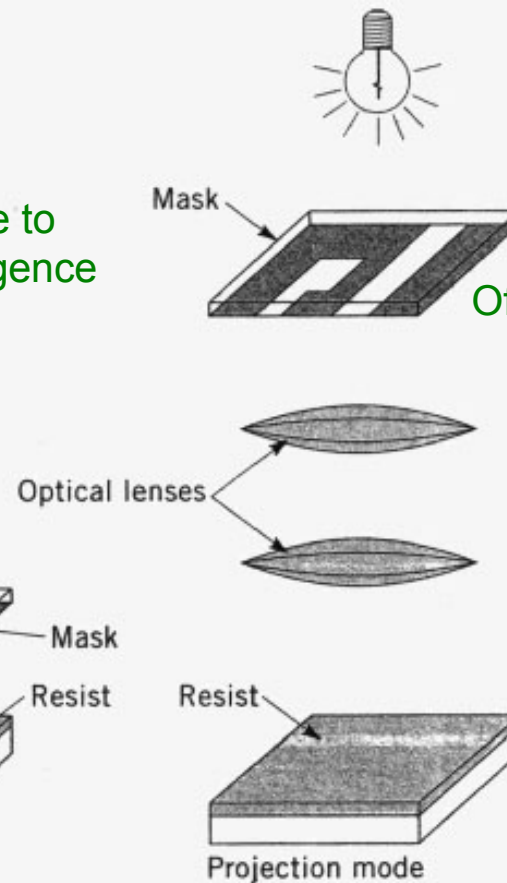
**Contact:**  
Good space definition  
but “interaction” problems



**Proximity**  
Highly sensitive to  
light beam divergence



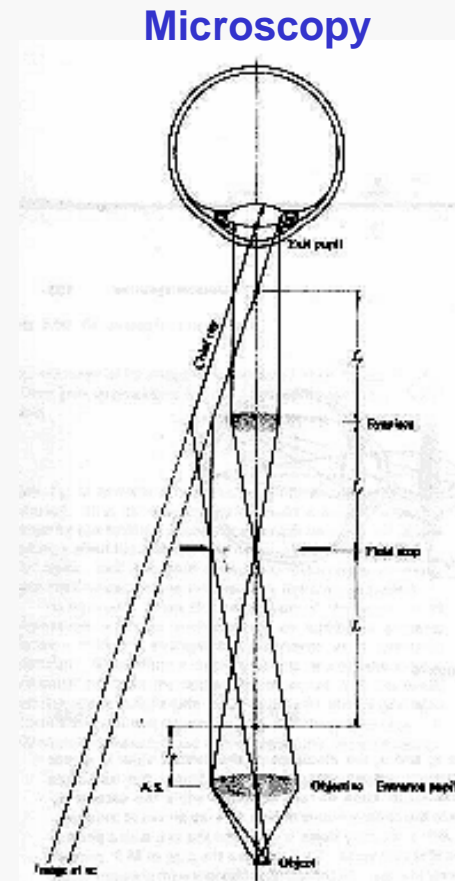
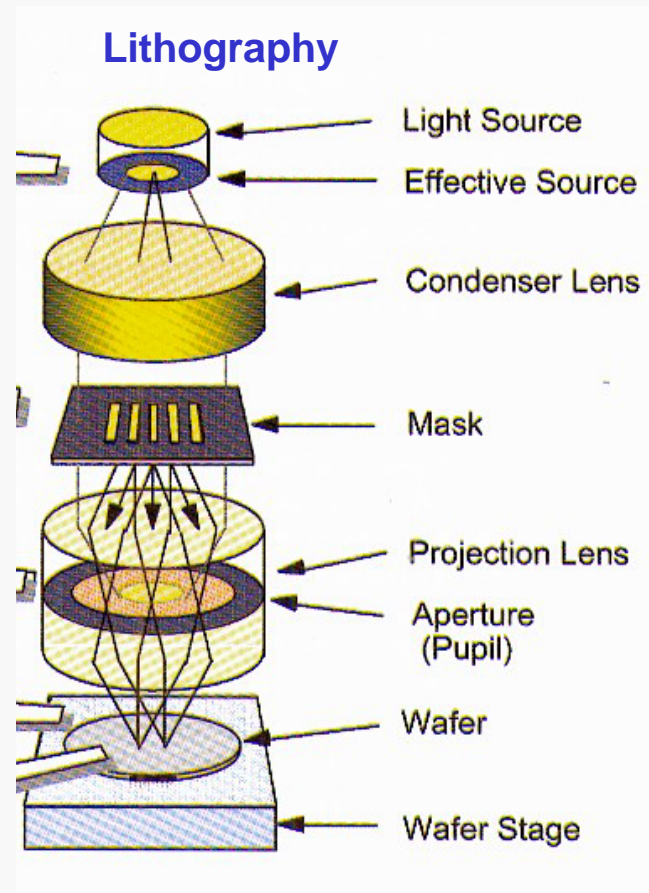
**Projection:**  
High flexibility  
Depends on optical quality  
Often used with step-and-repeat  
to cover large size wafers



Presently: **projection** modes are most common in industrial implementations, typically joined with “step and repeat” techniques (a small region of the substrate is impressed and then the substrate is moved to repeat the patterning over a larger area)

## 2. Complementarity lithography/microscopy

A system for optical projection lithography is clearly analogous to an optical microscope: location of light source and object are just reversed (indeed, this applies also to other lithography configurations!)



- Each microscopy method corresponds to a lithography approach
- Issues (as, e.g., spatial resolution) are common to the two topics



# Reminders on interference and diffraction

## 10.1.3 Several Coherent Oscillators

As a simple yet logical bridge between the studies of interference and diffraction, consider the arrangement of Fig. 10.6. The illustration depicts a linear array of  $N$  coherent point oscillators (or radiating antennas), which are each identical even to their polarization. For the moment, consider the oscillators to have no intrinsic phase difference, i.e. they each have the same epoch angle. The rays shown are all almost parallel, meeting at some very distant point  $P$ . If the spatial extent of the array is comparatively small, the separate wave amplitudes arriving at  $P$  will be essentially equal, having traveled nearly equal distances, that is

$$E_0(r_1) = E_0(r_2) = \dots = E_0(r_N) = E_0(r).$$

The sum of the interfering spherical wavelets yields an electric field at  $P$ , given by the real part of

$$E = E_0(r)e^{i(kr_1 - \omega t)} + E_0(r)e^{i(kr_2 - \omega t)} + \dots + E_0(r)e^{i(kr_N - \omega t)}. \quad (10.1)$$

It should be clear, from Section 9.1, that we need not be concerned with the vector nature of the electric field for this configuration. Now then

$$E = E_0(r)e^{-i\omega t}e^{ikr_1} [1 + e^{i(kr_2 - r_1)} + e^{i(kr_3 - r_1)} + \dots + e^{i(kr_N - r_1)}].$$

The phase difference between adjacent sources is obtained from the expression  $\delta = k_0\Lambda$  and since  $\Lambda = nd \sin \theta$ , in a medium of index  $n$ ,  $\delta = kd \sin \theta$ . Making use of Fig. 10.6, it follows that  $\delta = k(r_2 - r_1)$ ,  $2\delta = k(r_3 - r_1)$  etc. Thus the field at  $P$  may be written as

$$E = E_0(r)e^{-i\omega t}e^{ikr_1} [1 + (e^{i\delta}) + (e^{i\delta})^2 + (e^{i\delta})^3 + \dots + (e^{i\delta})^{N-1}]. \quad (10.2)$$

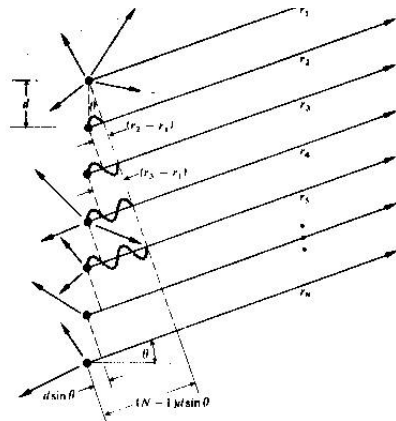


Fig. 10.6 A linear array of in-phase coherent oscillators. Note that at the angle shown  $\delta = \pi$  while at  $\theta = 0$   $\delta$  would be zero.

The bracketed geometric series has the value

$$(e^{i\delta N} - 1)/(e^{i\delta} - 1)$$

which can be rearranged into the form

$$e^{iN\delta/2} [e^{iN\delta/2} - e^{-iN\delta/2}] / [e^{i\delta/2} - e^{-i\delta/2}]$$

or equivalently

$$e^{i(N-1)\delta/2} \left[ \frac{\sin N\delta/2}{\sin \delta/2} \right]$$

The field then becomes

$$E = E_0(r)e^{-i\omega t}e^{i(kr_1 - \omega t)} e^{i(N-1)\delta/2} \left( \frac{\sin N\delta/2}{\sin \delta/2} \right). \quad (10.3)$$

Notice that if we define  $R$  to be the distance from the center of the line of oscillators to the point  $P$ , that is

$$R = \frac{1}{2}(N-1)d \sin \theta + r_1,$$

then Eq. (10.3) takes on the form

$$E = E_0(r)e^{i(kR - \omega t)} \left( \frac{\sin N\delta/2}{\sin \delta/2} \right). \quad (10.4)$$

Finally, then, the flux-density distribution within the diffraction pattern due to  $N$  coherent, identical, distant point sources in a linear array is proportional to  $EE^*/2$  for complex  $E$  or

$$I = I_0 \frac{\sin^2 (N\delta/2)}{\sin^2 (\delta/2)}. \quad (10.5)$$

where  $I_0$  is the flux density from any single source arriving at  $P$  (see Problem 10.2 for a graphical derivation of the irradiance). For  $N = 0$ ,  $I = 0$ , for  $N = 1$ ,  $I = I_0$ , and for  $N = 2$ ,  $I = 4I_0 \cos^2 (\delta/2)$  in accord with Eq. (9.6). The functional dependence of  $I$  on  $\theta$  is more apparent in the form

$$I = I_0 \frac{\sin^2 [N(kd/2) \sin \theta]}{\sin^2 [(kd/2) \sin \theta]}. \quad (10.6)$$

The  $\sin^2 [N(kd/2) \sin \theta]$  term undergoes rapid fluctuations, while the function modulating it,  $\{\sin [(kd/2) \sin \theta]\}^{-2}$ , varies relatively slowly. The combined expression gives rise to a series of sharp principal peaks separated by small subsidiary maxima. The principal maxima occur in directions  $\theta_m$  such that  $\delta = 2m\pi$  where  $m = 0, \pm 1, \pm 2, \dots$ . Because  $\delta = kd \sin \theta$

$$d \sin \theta_m = m\lambda. \quad (10.7)$$

Since  $[\sin^2 N\delta/2]/[\sin^2 \delta/2] = N^2$  for  $\delta = 2m\pi$  (from

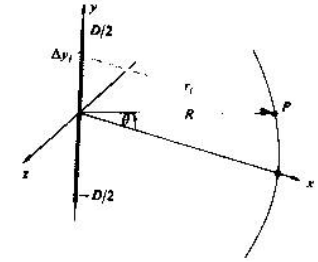


Fig. 10.8 A coherent line source.

L'Hôpital's rule) the principal maxima have values  $N^2 I_0$ . This is to be expected inasmuch as all of the oscillators are in phase at that orientation. The system will radiate a maximum in a direction perpendicular to the array ( $m = 0, \theta_0 = 0$  and  $\pi$ ). As  $\theta$  increases,  $\delta$  increases and  $I$  falls off to zero at  $N\delta/2 = \pi$ , its first minimum. Note that if  $d < \lambda$  in Eq. (10.7), only the  $m = 0$  or zero-order principal maximum exists. *If we were looking at an idealized line source of electron-oscillators separated by atomic distances, we could expect only that one principal maximum in the light field.*

The antenna array of Fig. 10.7 can then transmit radiation in the narrow beam or lobe corresponding to a principal maximum (the parabolic dishes shown reflect into the forward direction and the radiation pattern is no longer symmetrical around the common axis.) Suppose that we have a system in which we can introduce an intrinsic phase shift of  $\epsilon$  between adjacent oscillators. In that case

$$\delta = kd \sin \theta + \epsilon;$$

the various principal maxima will occur at new values

$$d \sin \theta_m = m\lambda - \epsilon/k.$$

Concentrating on the central maximum  $m = 0$ , its orientation  $\theta_0$  can be varied at will by merely adjusting the value of  $\epsilon$ .

The principle of reversibility, which states that without absorption, wave motion is reversible, leads to the same field pattern for an antenna used as either a transmitter or receiver. The array, functioning as a radio telescope, can therefore be "pointed" by combining the output from the individual antennas with an appropriate phase shift,  $\epsilon$ , introduced

between each of them. For a given  $\epsilon$  the output of the system corresponds to the signal impinging on the array from a specific direction in space.

Figure 10.7 is a photograph of the first multiple radio interferometer designed by W. N. Christiansen and built in Australia in 1951. It consists of 32 parabolic antennas, each 2 m in diameter, designed to function in phase at the wavelength of the 21 cm hydrogen emission line. The antennas are arranged along an east-west baseline with 7 m separating each one. This particular array utilizes the earth's rotation as the scanning mechanism.

Examine Fig. 10.8 which depicts an idealized line source of electron-oscillators (e.g., the secondary sources of the Huygens-Fresnel principle for a long slit whose width is much less than  $\lambda$  illuminated by plane waves). Each point emits a spherical wavelet which we write as

$$E = \left( \frac{\mathcal{E}_0}{r} \right) \sin(\omega t - kr)$$

explicitly indicating the inverse  $r$ -dependence of the amplitude. The quantity  $\mathcal{E}_0$  is said to be the *source strength*. The present situation is distinct from that of Fig. 10.6 in that now the sources are very weak, their number,  $N$ , is tremendously large and the separation between them vanishingly small. A minute, but finite segment of the array  $\Delta y_i$ , will contain  $\Delta y_i(N/D)$  sources where  $D$  is the entire length of the array.

# Fraunhofer diffraction

Imagine then that the array is divided up into  $M$  such segments, i.e.,  $i$  goes from 1 to  $M$ . The contribution to the electric field intensity at  $P$  from the  $i$ th segment is accordingly

$$E_i = \left( \frac{\mathcal{E}_0}{r_i} \right) \sin(\omega t - kr_i) \left( \frac{N \Delta y_i}{D} \right)$$

provided that  $\Delta y_i$  is so small that the oscillators within it have a negligible relative phase difference ( $r_i = \text{constant}$ ) and their fields simply add constructively. We can cause the array to become a continuous (coherent) line source by letting  $N$  approach infinity. This description, besides being fairly realistic on a macroscopic scale, also allows the use of the calculus for more complicated geometries. Certainly as  $N$  approaches infinity, the source strengths of the individual oscillators must diminish to near zero if the total output is to be finite. We can therefore define a constant  $\mathcal{E}_L$  as the *source strength per unit length* of the array, that is

$$\mathcal{E}_L \equiv \frac{1}{D} \lim_{N \rightarrow \infty} (\mathcal{E}_0 N). \quad (10.8)$$

The net field at  $P$  from all  $M$  segments is

$$E = \sum_{i=1}^M \frac{\mathcal{E}_L}{r_i} \sin(\omega t - kr_i) \Delta y_i.$$

For a continuous line source  $\Delta y_i$  can become infinitesimal ( $M \rightarrow \infty$ ) and the summation is then transformed into a definite integral

$$E = \mathcal{E}_L \int_{-D/2}^{+D/2} \frac{\sin(\omega t - kr)}{r} dy. \quad (10.9)$$

where  $r = r(y)$ . The approximations used to evaluate Eq. (10.9) must depend on the position of  $P$  with respect to the array and will therefore make the distinction between Fraunhofer and Fresnel diffraction. The coherent *optical* line source does not now exist as a physical entity but we will make good use of it as a mathematical device.

## 10.2 FRAUNHOFER DIFFRACTION

### 10.2.1 The Single Slit

Return to Fig. 10.8 where now the point of observation is very distant from the coherent line source and  $R \gg D$ . Under these circumstances  $r(y)$  never deviates appreciably from its midpoint value  $R$  so that the quantity  $(\mathcal{E}_L/R)$  at  $P$  is essentially constant for all elements  $dy$ . It follows from Eq. (10.9) that the field at  $P$  due to the differential segment of the

source  $dy$  is

$$dE = \frac{\mathcal{E}_L}{R} \sin(\omega t - kr) dy, \quad (10.10)$$

where  $(\mathcal{E}_L/R) dy$  is the amplitude of the wave. Notice that the phase is very much more sensitive to variations in  $r(y)$  than is the amplitude so that we will have to be more careful about introducing approximations into it. We can expand  $r(y)$ , in precisely the same manner as was done in Problem (9.4), to get it as an explicit function of  $y$ , thus

$$r = R - y \sin \theta + (y^2/2R) \cos^2 \theta + \dots, \quad (10.11)$$

where  $\theta$  is measured from the  $xz$ -plane. The third term can be ignored so long as its contribution to the phase is insignificant even when  $y = \pm D/2$ , i.e.,  $(\pi D^2/4\lambda R) \cos^2 \theta$  must be negligible. This will be true for all values of  $\theta$  when  $R$  is adequately large and we again have the Fraunhofer condition. The distance  $r$  is then linear in  $y$ . Substituting into Eq. (10.10) and integrating leads to

$$E = \frac{\mathcal{E}_L}{R} \int_{-D/2}^{+D/2} \sin[\omega t - k(R - y \sin \theta)] dy, \quad (10.12)$$

and finally

$$E = \frac{\mathcal{E}_L D \sin[(kD/2) \sin \theta]}{R (kD/2) \sin \theta} \sin(\omega t - kR). \quad (10.13)$$

To simplify the appearance of things let

$$\beta \equiv (kD/2) \sin \theta \quad (10.14)$$

so that

$$E = \frac{\mathcal{E}_L D}{R} \left( \frac{\sin \beta}{\beta} \right) \sin(\omega t - kR). \quad (10.15)$$

The quantity most readily measured is the irradiance (forgetting the constants)  $I(\theta) = \langle E^2 \rangle$  or

$$I(\theta) = \frac{1}{2} \left( \frac{\mathcal{E}_L D}{R} \right)^2 \left( \frac{\sin \beta}{\beta} \right)^2, \quad (10.16)$$

where  $\langle \sin^2(\omega t - kR) \rangle = \frac{1}{2}$ . When  $\theta = 0$ ,  $\sin \beta/\beta = 1$  and  $I(\theta) = I(0)$  which corresponds to the *principal maximum*. The irradiance resulting from an idealized coherent line source in the Fraunhofer approximation is then

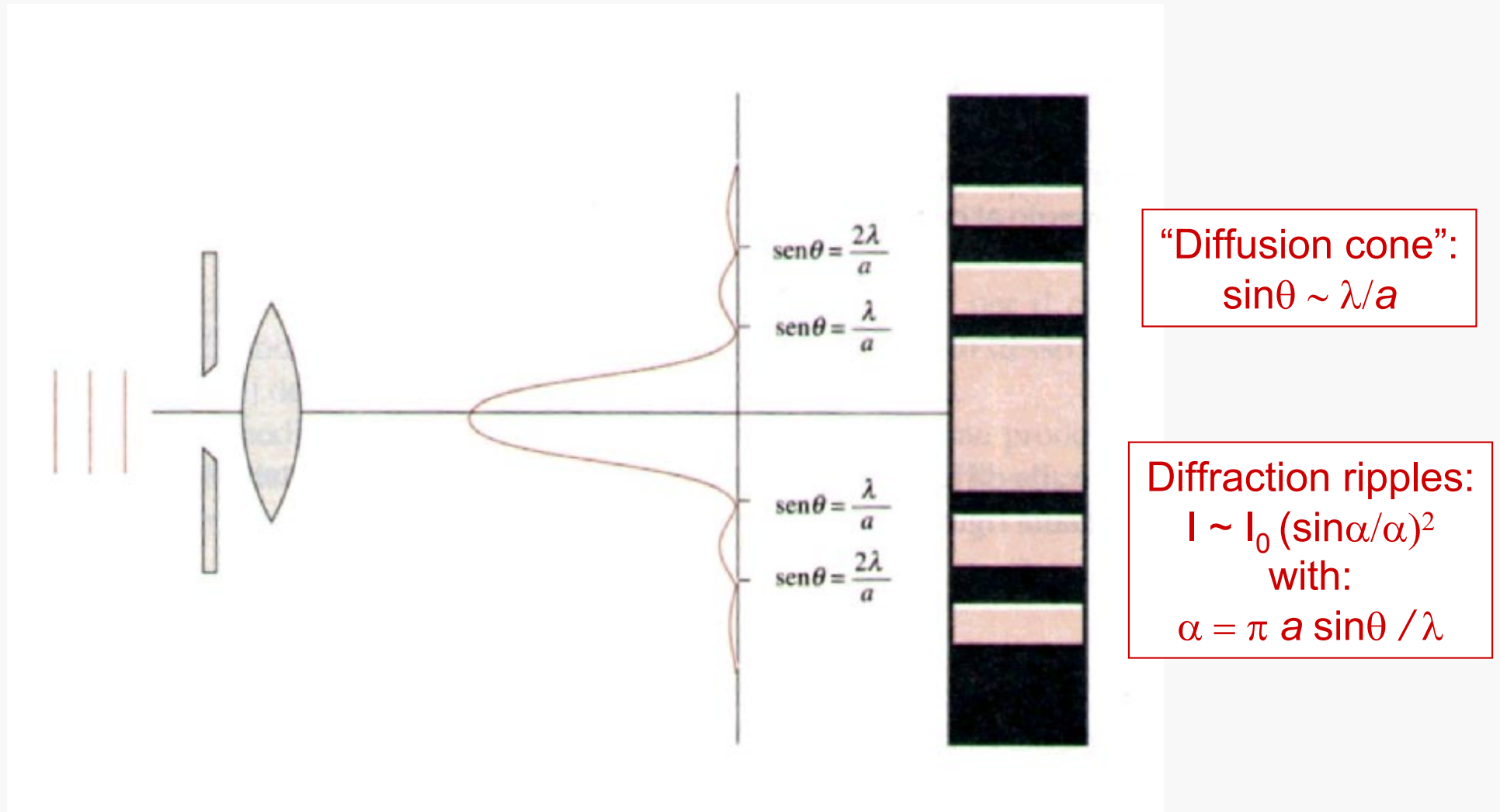
$$I(\theta) = I(0) \left( \frac{\sin \beta}{\beta} \right)^2, \quad (10.17)$$

or using the *sinc function* (Section 7.9, and Table 1 of the Appendix)

$$I(\theta) = I(0) \text{sinc}^2 \beta.$$

There is symmetry about the  $y$ -axis and this expression holds for  $\theta$  measured in any plane containing that axis.

## Effects of diffraction



**Optical diffraction is for sure a *fundamental* limiting factor in optical lithography**

# Criteria for space resolution (in optical microscopy)

## 3.1.2.1 POINT-SOURCE ABBE IMAGE

The calculated intensity distribution assumes a parallel beam of light travelling along the axis of a thin lens and brought to a focus at the focal distance (Fig. 3.8). For the *cylindrically symmetric* case, the ratio of the peak intensities for the primary and secondary peaks in the intensity distribution is *ca* 9:1, while the width of the primary peak is given by the *Abbe equation* as follows:

$$\delta = 0.61 \frac{\lambda}{\mu \sin \alpha} \quad \text{Abbe} \quad (3.1)$$

where  $\lambda$  is the wavelength of the radiation,  $\alpha$  is the aperture (half-angle) of the lens (determined by the ratio of the lens radius to its focal length), and  $\mu$  is the refractive index of the medium between the lens and the focal point ( $\mu \approx 1$  for air).

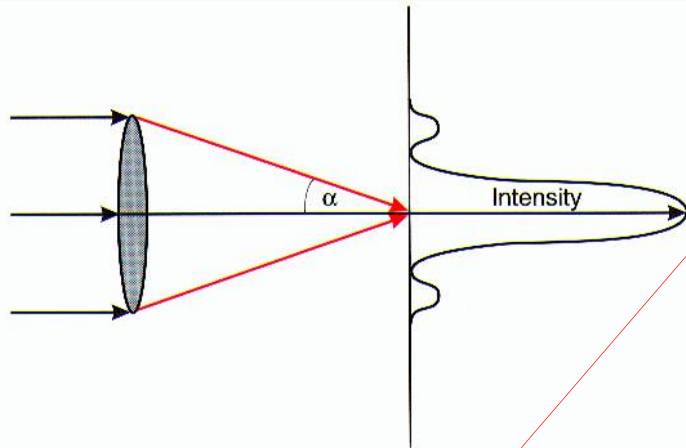
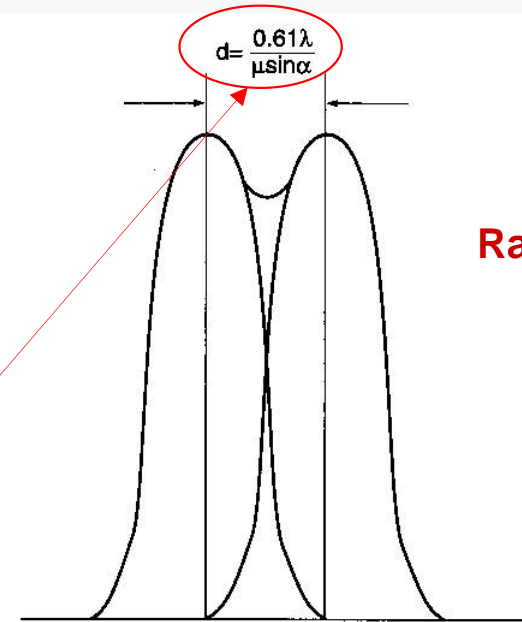


Figure 3.8 The Abbe equation gives the width of the first intensity peak for the image of point object at infinity in terms of the angular aperture of the lens  $\alpha$  and the wavelength of radiation  $\lambda$ .



Rayleigh

Figure 3.10 The Rayleigh resolution criterion requires that two point sources at infinity have an angular separation which is sufficient to place the maximum intensity of the primary image peak of one source at the position of the first minimum of the second

Da Brandon Kaplan  
Microstruct. Charact.  
of Materials  
Wiley (1999)

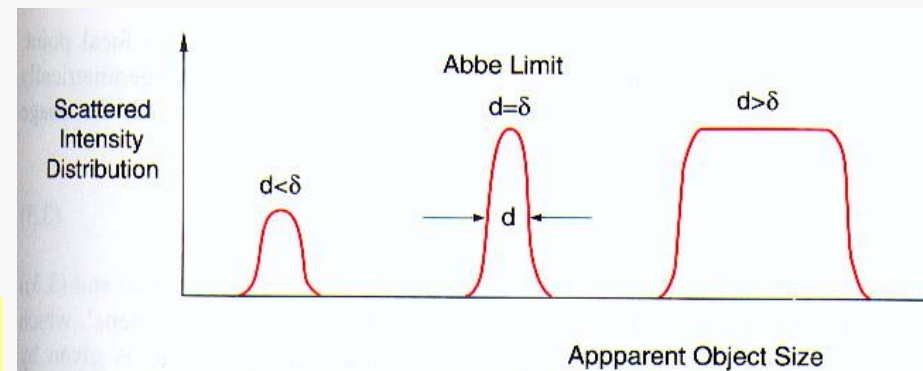


Figure 3.11 Large objects of diameter  $d$  are blurred by the diffraction limit  $\delta$  derived from the Abbe relationship, but objects smaller than the Abbe width are still detectable in the microscope, although the intensity is reduced and they have an apparent width given by the Abbe equation

**Maximum achievable space resolution  $d \sim 0.61 \lambda / (NA) < \lambda / 2$  (NA: numerical aperture of the optical system)**

# Optical confocal microscopy I

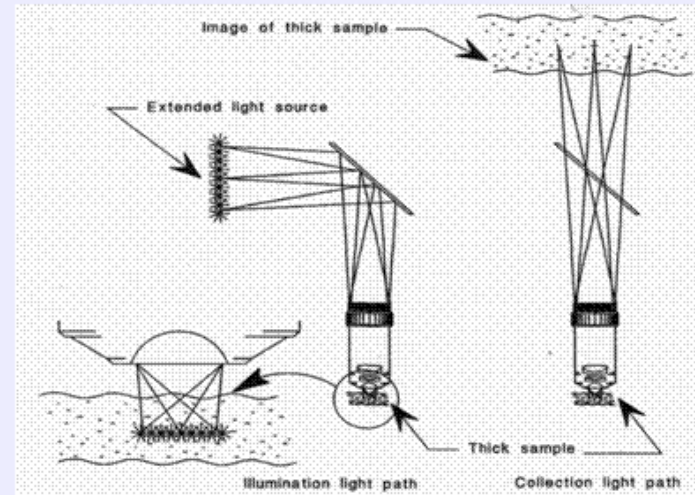
In practical terms, space resolution is also a matter of contrast

In all microscopies, methods exist to improve the contrast, so enhancing the resolution

For instance, in optical microscopy **confocal** systems have been developed with a space resolution on the order of 200 nm (for the visible light)

“Stray light” effects are removed and the contrast is enhanced

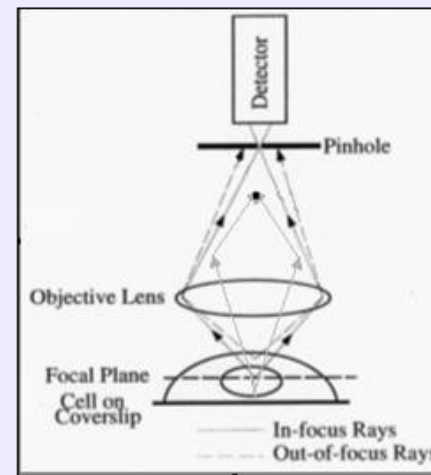
## Extended Light Versus Point Light Source Illumination



In conventional wide field microscope, ordinary extended light is used as light source, the specimen is lit laterally and vertically at the same time as shown in the illustration. The resulting image is affected by all the lit spots from the whole illuminated field, although it is centered at a given focal plane and local spot. These illuminated dots interfere with each other laterally and the stray light compromise image contrast. Image contrast, defined as the difference between the

minimum and maximum intensity of two points in the image, is an important factor for an optical device to achieve its resolution, without proper contrast, the signal has little difference with background and the resolution of the an optical lens can not be realized. Improved contrast helps an optical device to reach its maximum resolution.

In another configuration, a plate with a small hole called pinhole is placed before the image detecting device like below:



In this configuration, light from under-focal-plane will be focused at a plane behind the pinhole such is blocked away by the pinhole plate. The light from above-focal-plane will be focused before the pinhole and is blocked away by the pinhole too. Only the light from focal plane is just focused at the pinhole thus can reach the image detector. This process simulates what you do with a microtome to cut some unwanted tissue away, but you do it here optically, this is so called "**optical sectioning**".

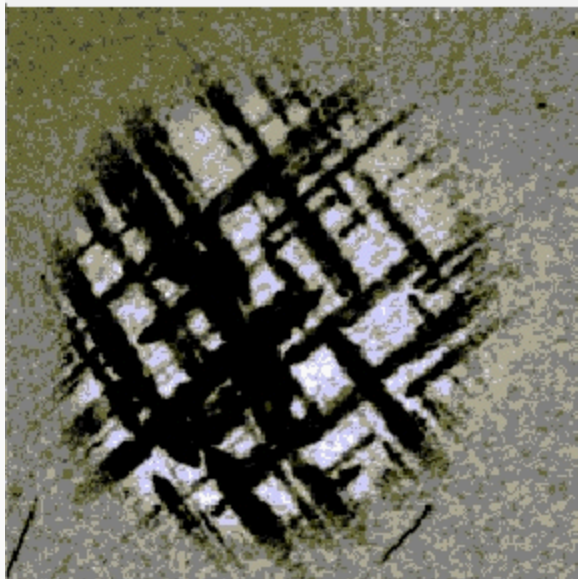
The size of pinhole determines how thick an optical slice will be. The smaller the pinhole, the thinner the slice. But the thickness will not go down indefinitely. It is also limited by all those factors affecting resolution of the lens: the wave length of light, Numerical aperture of the lens, reflecting index of media, together with pinhole size, the z-resolution is usually 2 times worse than lateral resolution of an objective. For a lens of 1.4 NA, blue light at 488 nm, the lateral resolution is 200 nm, the achievable optical section thickness is about 400 nm.

# Optical confocal microscopy II

Confocal microscopy often used for biological samples with fluorescent markers (e.g., quantum dots)

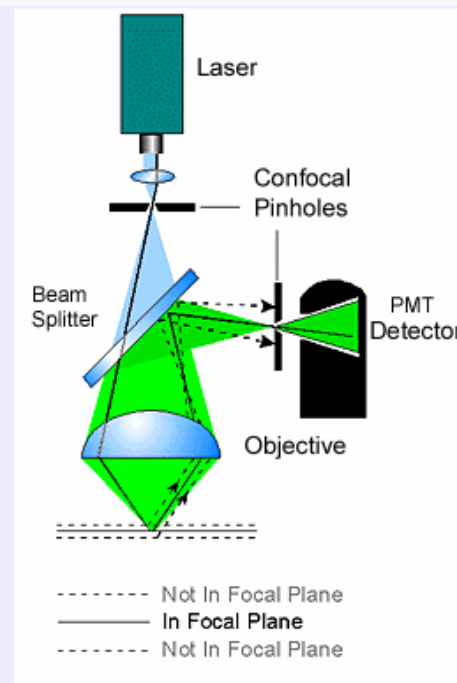
3D mapping capabilities can be added by moving the system along the focal axis

Frequently 2-photon excitation is used to further enhance space resolution (due to the nonlinear dependence of the absorption probability on the exciting intensity)



“Segregation” of quantum wells

Confocal photoluminescence images of a II-VI laser structure showing ZnCdSe/ZnSSe/ZnMgSSe separate confinement heterostructure:



In practical, a point-like light source is achieved by using a laser light passing through a illumination pinhole. This point-like light source is directed to the specimen by a beam splitter (or AOBS in Leica's BSP-free system) to form a point-like illumination in the specimen. The point-illumination move or scan the specimen by the help of a scanner. The reflected emission light from specimen's focal plane passes through the detecting pinhole and form point-like image on detector PMT (photon multiply tube).

PMT converts detected photon into electron. It is possible to amplify weak signal by manipulating the voltage (gain) on the tube. It is also possible to cut off background signal by set certain threshold (Offset) on the tube.

PMT has large active area to receive photons thus high saturate point, and PMT has low dark current thus low background, together, which provide high dynamic range that is defined as the ratio of maximum allowed intensity / dark current. Besides, PMT has very high refresh rate since there is no charge accumulate on it. It detects event at nano- seconds level.

Taking together, in confocal system:

- A point light source for illumination
- A point light focus within the specimen
- A pinhole at the image detecting plane

These **three points** are **optically conjugated together** and aligned accurately to each other in the light path of image formation, this is **confocal**. Confocal effects result in suppression of out-of-focal-plane light, suppression of stray light in the final image

Confocal images have following features:

- void of interference from lateral stray light: higher contrast.
- void of superimpose of out-of-focal-plane signal: less blur, sharper image.
- images derived from optically sectioned slices (depth discrimination)
- Improved resolution (theoretically) due to better wave-optical performance.

**Is confocal effect a free cake?**

No, confocal effect is obtained at a cost of greatly reduced detecting volume (total signal amount), increase vulnerability to noise, reduced dynamic range, etc. For detailed discussion, refer section 6: [Optical sectioning](#).

# Space resolution in optical lithography I

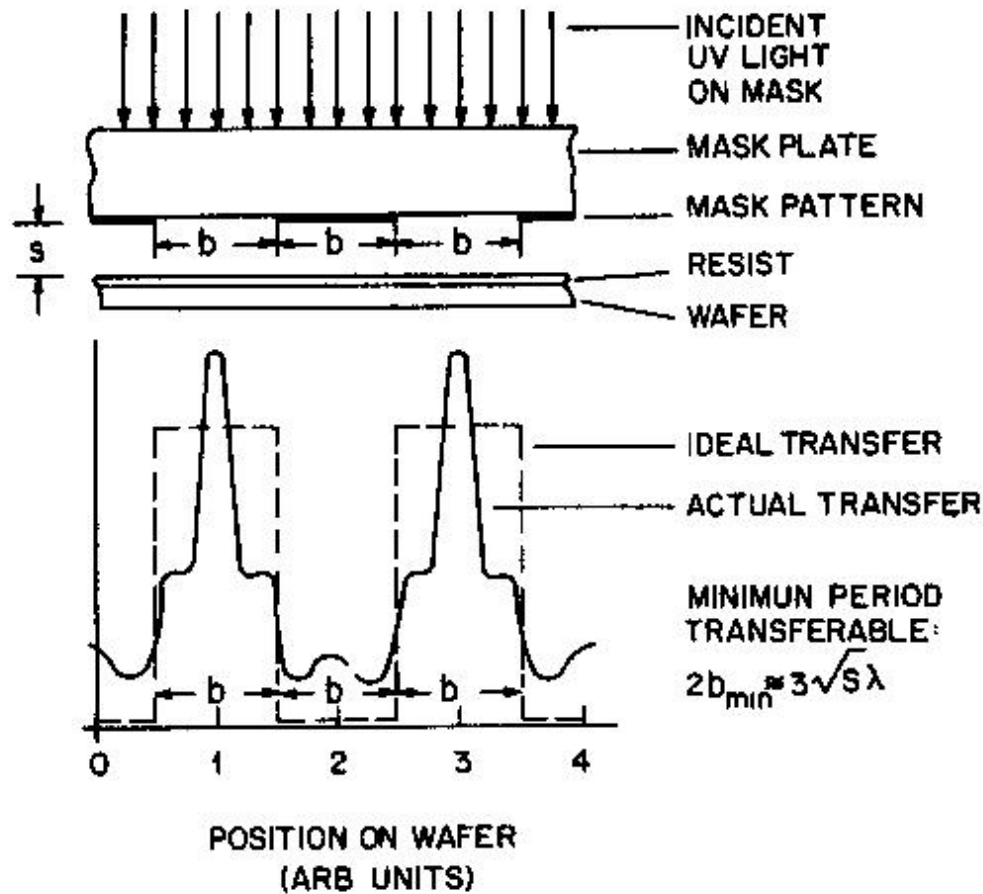


**Figure 1.7** Light distribution profiles on a photoresist surface after light passed through a mask containing an equal line and space grating. (From Willson, C. G., in *Introduction to Microlithography*, Thompson, L. F., Willson, C. G., and Bowden, M. J., Eds., American Chemical Society, Washington, D.C., 1994. With permission.)

Further *technological* limitations:  
 Mask/substrate distance (divergence);  
 Resist thickness and depth of field;  
 Resist homogeneity

**Empirical formula:**

$$2b_{\min} = 3\sqrt{\lambda\left(s + \frac{Z}{2}\right)} \quad 1.12$$

where  $b_{\min}$  stands for half the grating period,  $s$  for the gap between the mask and the photoresist surface,  $\lambda$  for the wavelength of the exposing radiation, and  $z$  for the photoresist thickness.

Example:

$\lambda = 350 \text{ nm}$ ,  $s = 5 \text{ }\mu\text{m}$ ,  $Z = 0.5 \text{ }\mu\text{m}$   
 $\rightarrow b_{\min} > 2 \text{ }\mu\text{m}!!!$

**Care must be put even to approach the diffraction limit**

# Space resolution II

## 2 Optical Lithography

Optical lithography is the most important type of lithography. Originally the name referred to lithography using light with wavelength in the visible range. Nevertheless, gradually, the wavelength was driven down to 193 nm, which is used in semiconductor production nowadays, and even shorter wavelengths down to the sub-nm range are under investigation.

The key issue of lithography is the resolution of the system, and hence the size of the smallest feature (minimum feature size: *MFS*) which can be defined on the sample. This *MFS* depends on the illumination method, the illumination wavelength  $\lambda$ , on the materials of the optical system and the resist used. In Sec. 2.1 the different illumination methods and their physical resolution limits are addressed, in Sec. 2.2 the wavelengths and the light sources are discussed, also for wavelengths below 15 nm, while lithography with these wavelengths is discussed in Sec. 3 and 4, and in Sec. 2.3 the materials and the forms of the optical system are dealt with.

### 2.1 Illumination Methods and Resolution Limits

Figure 3 shows a schematic view of the three different illumination methods *contact*, *proximity* and *projection lithography*. With all three, the light emitted by a light source passes a condenser optics so that a parallel beam is formed. With contact lithography, mask and sample are pressed together so that the mask is in close contact to the resist (Figure 3a). The resolution is limited by deflection and is expressed by the *MFS* which can be obtained. For contact lithography this is  $MFS = \sqrt{d \cdot \lambda}$ , where  $d$  is the resist thickness and  $\lambda$  the wavelength. For a resist thickness of 1  $\mu\text{m}$  and a wavelength of about 400 nm, this yields a minimum feature size of 600 nm. The major drawback of this method is that the quality of the mask suffers from contact to the resist, leading to failures in the structure. To avoid this problem, the second method was developed (Figure 3b). With *proximity lithography* there is a defined proximity gap  $g$  between sample and mask, so there is no deterioration of the mask. The drawback is the poorer resolution limit, which is proportional to  $\sqrt{(d+g) \cdot \lambda}$ . With same figures as above and a proximity gap of 10  $\mu\text{m}$ , the *MFS* is 2  $\mu\text{m}$ .

The method used today in industrial production is so-called *projection lithography* (Figure 3c). Here not the shadow of the mask is transferred to the sample as with the two other methods, but a picture of the mask is projected onto the sample. Therefore after passing the mask, the light is bundled by an optical system. The mask is not in contact with the sample, so there is no deterioration as in contact lithography, but the resolution is better than in proximity lithography. Furthermore it is possible to reduce the picture so the patterns on the mask are allowed to be bigger than the patterns on the sample. This is

advantageous for mask fabrication: Errors are also reduced. If it is possible to obtain masks with an accuracy of 100 nm, then the error for a structure of 500 nm to be transferred onto a sample is 20 %, if it is transferred one by one. If the picture is reduced 4 times, then for a 500 nm feature on the sample, the feature on the mask has to be 2  $\mu\text{m}$ ; therefore the mask error is only 5 %. Because of the reduction, the wafer is not exposed in one exposure, but in several. This is done by so-called steppers, in which the wafer is adjusted under the mask by an x-y-table. The stepper moves the wafer from one exposure position to the next, while the mask is not moved.

in projection lithography the limiting factor to the *MFS* is diffraction. Consider a slit width  $b$  which is illuminated by a monochromatic plane wave. What will the intensity distribution look like on a screen at a distance  $l$  behind the slit? Therefore consider two Huygens waves, one from the lower rim of the slit, one from the middle. There will be an optical path difference between these two Huygens waves, depending on the angle of propagation  $\Theta$ . The magnitude of the path difference (*PD*) is:

$$PD = \frac{b}{2} \sin(\Theta) \quad (1)$$

The two Huygens waves will interfere destructively if the *PD* is an odd multiple of the half wavelength:

$$\frac{b}{2} \sin(\Theta_{\min}) = (2m+1) \cdot \frac{\lambda}{2} \quad \text{with } m = 0, \pm 1, \pm 2, \dots \quad (2)$$

Under this condition, the Huygens waves from the lower part of the slit will interfere destructively with the ones from the upper part. At the angle  $\Theta_{\min}$  there is a minimum of intensity.

The Huygens waves do interfere constructively resulting in a maximum of intensity when:

$$\frac{b}{2} \sin(\Theta_{\max}) = m\lambda \quad \text{with } m = 0, \pm 1, \pm 2, \dots \text{ holds.} \quad (3)$$

In lithography the diffraction patterns of several structures are superimposed so the question leading to the *MFS* is the question of when two structures can be resolved. The first approach is given by the Rayleigh criterion [3]. When light coming from a point source passes an optical system a blurred diffraction pattern – the Airy disc – occurs. The Rayleigh criterion says that two ideal point sources (e.g. stars) can be resolved when the intensity maximum of the one Airy disc is in the first minimum of the other, so *MFS* is given as:

$$MFS = 0.61 \cdot \frac{\lambda}{NA} \quad (4)$$

where  $NA$  is the numerical aperture of the optical system. Nevertheless the Rayleigh criterion is just a first approach to the *MFS* in microlithography. The mask patterns are not independent (i.e. incoherent) ideal point sources, on the contrary they have a finite width and the light is partially coherent. Nevertheless, the form of the criterion gives the right dependences. If the wavelength is decreased by 10 % or the  $NA$  is increased by 10 %, the *MFS* is improved by 10 %. Furthermore, it was derived only by properties of the optics although the photoresist also affects the *MFS*. Therefore more generally, the criterion is written as:

$$MFS = k_1 \cdot \frac{\lambda}{NA} \quad (5)$$

where  $k_1$  is a constant (typically 0.5 – 0.9), which accounts for non-ideal behaviour of the equipment (e.g. lens errors) and the influences which do not come from the optics (resist, resist processing, shape of the imaged structures,...). Therefore  $k_1$  is called the technology constant.

As a comparison, for a technology constant of 0.7 and a numerical aperture of 0.7, which are commonly used figures, the *MFS* is in the order of the wavelength  $\lambda$ . So it is better by about a factor of 0.66 than the *MFS* of contact printing.

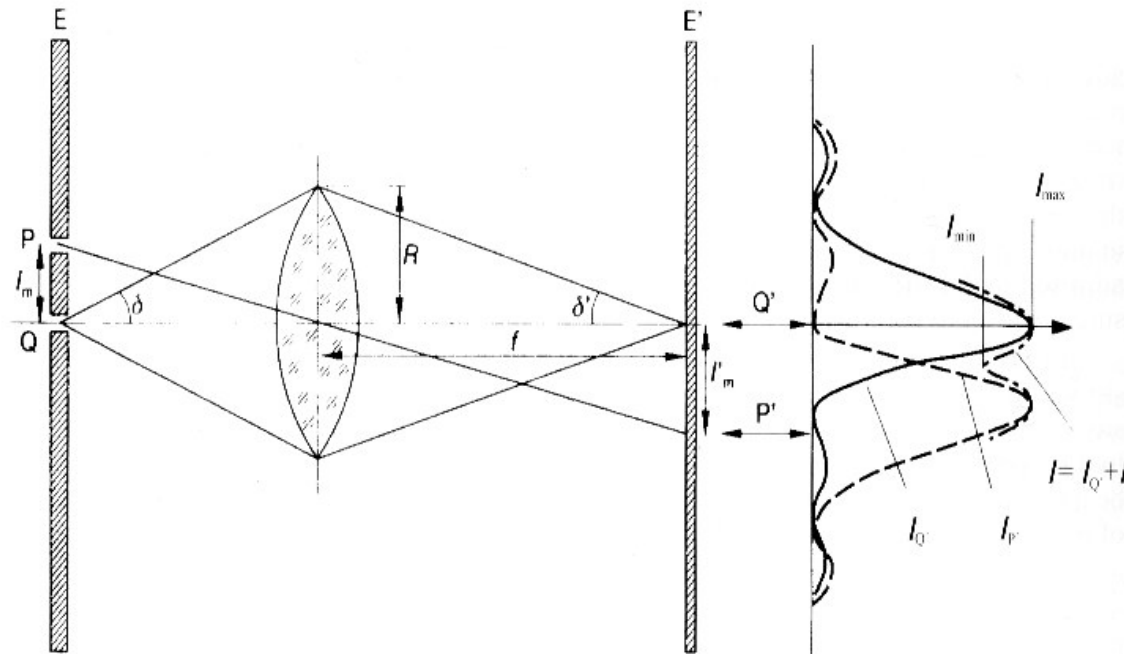
# Space resolution III

Figure 4 clarifies the connection between mask, diffraction and intensity distribution in the image plane. Due to diffraction two sharp features, P and Q, on the mask give rise to an overall intensity distribution on the sample. To resolve these two features the intensity distribution has to have a minimum between the two main maximums. It is useful to define the so called modulation transfer function (*MTF*) as:

$$MTF = \frac{I_{\max} - I_{\min}}{I_{\max} + I_{\min}} \quad (6)$$

The higher the value – the higher the difference between the maximum and minimum intensity – the better the contrast between exposed and unexposed areas, the better is the resolution of the equipment. It should be noted that the *MTF* is only derived by properties of the optical system. It is a measure of the capabilities of the lithographic tool in printing structures.

**Pattern contrast affected by optical diffraction**



# 3. Strategies to improve resolution I: phase shift masks

## Resolution Enhancement Technologies

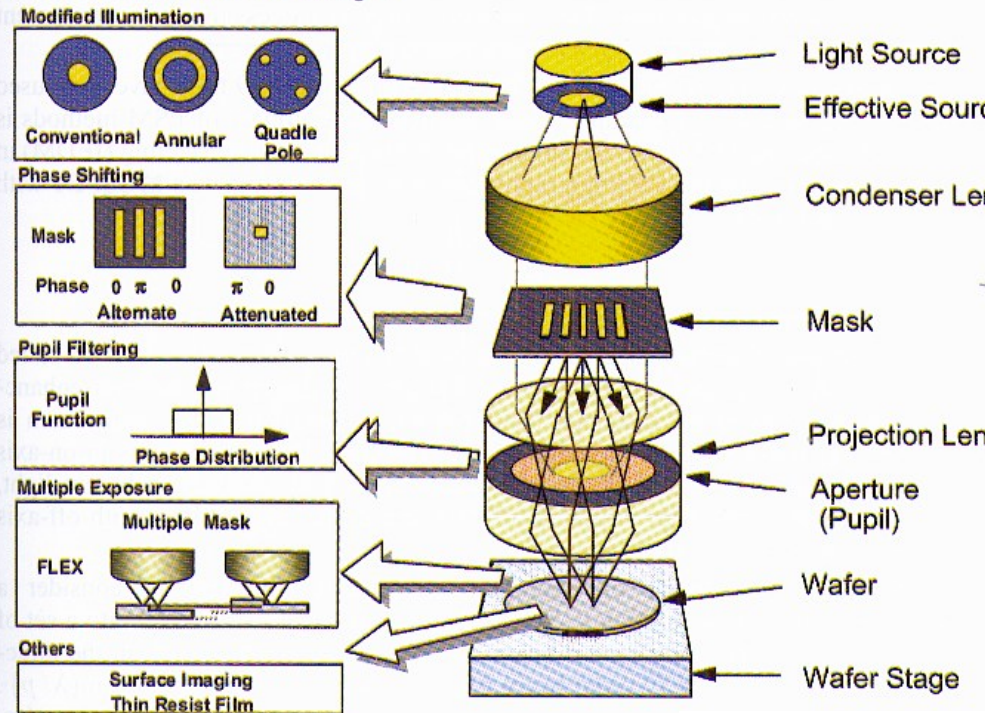
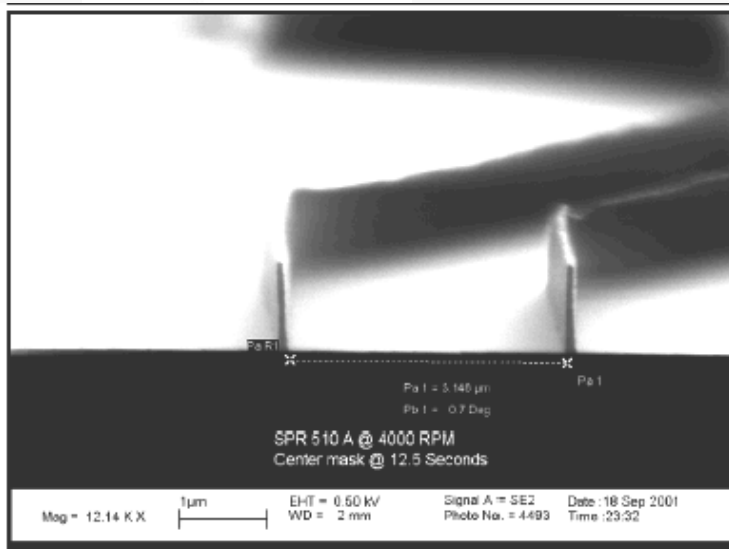


Figure 5: Survey of the resolution enhancement techniques.



Example: features ~ 100 nm made with 350 nm radiation

so-called *Levenson* or *alternating phase shift masks* (PSM) can improve the resolution by 40%. Unfortunately, this improvement is pattern-dependent; for a single structure there is no neighboring structure, so there is no light to interfere with. Even if there are structures which are not in a regular arrangement, there is no defined phase shift between these structures which could yield an improvement in the resolution of all structures.

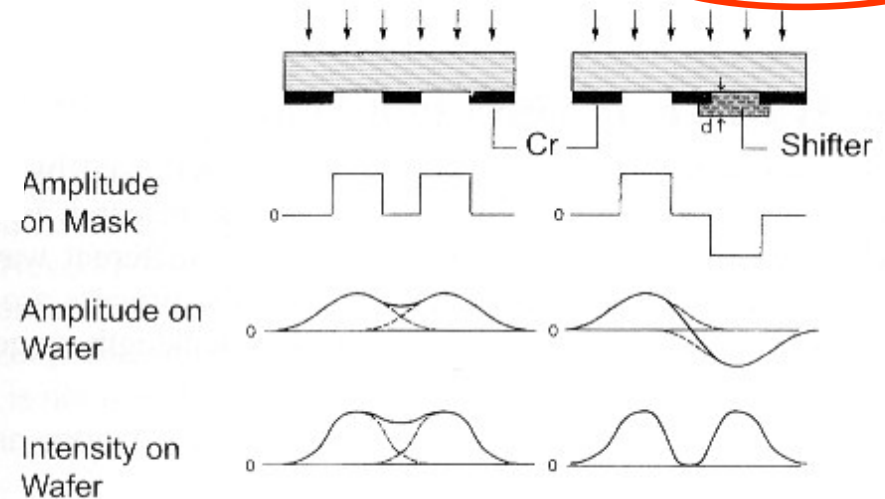
The phase shift can be obtained by an additional transparent layer on the mask. If it has the refractive index  $n$  and thickness  $d$ , the phase shift is  $\Phi = (n-1)2\pi d/\lambda$ . So a shift of  $\pi$  is obtained, when the condition  $d = \lambda/[2(n-1)]$  holds. On the other hand, it is also possible to recess the mask material so that the right optical path difference is obtained. But the etch depth can be controlled by the time only, and not, as in etching away an additional layer, by the thickness of the layer itself.

To deal with the drawbacks of alternating PSM, several other methods have been developed, which are described next. In rim-PSM, the whole mask is covered by a phase-shifter material and then with the resist. After development, the phase shifter is etched anisotropically and the masking layer is etched isotropically. By this a undercut under the phase shifter occurs at the rim of every structure. This also yields a resolution improvement, but not as much as with alternating PSM, although it is therefore not limited to certain structures.

Figure 6: Comparison of the light amplitudes and intensities at the mask and on the wafer for a conventional and a phase shift mask. Note that the intensity on the wafer between the two features is zero for the phase shift mask [26].

Conventional Mask

Phase Shift Mask



# Strategies to improve resolution II: off-axis illumination

## Off-Axis Illumination

To improve resolution without decreasing the wavelength or increasing  $NA$ , so-called off-axis illumination was applied. The method was already known as a contrast-enhancing technique for optical microscopes. With off-axis illumination, the light beam is directed from the mask towards the edge of the projection lens, and not, as in on-axis illumination, towards the center. In normal illumination with partially coherent light, there always is part of the light which is off-axis, but in the context here with off-axis illumination there is no on-axis component.

To understand the mode of operation of off-axis illumination, consider a line-and-spaces structure with pitch  $p$ . The incident light will be diffracted into a set of beams, of which only the undiffracted beam, the zero-order beam, travels in the direction of the incident light. The 1<sup>st</sup> order beam travels under the angle  $|\theta_1| = \arcsin(\lambda/p)$ . If  $p$  is too small, then  $|\theta_{\pm 1}|$  is bigger than the acceptance angle  $\alpha$  of the projection optics, then only the zero-order beam is projected to the sample (Figure 7a). But this does not carry any information of the pattern, and hence the pattern cannot be transferred onto the sample. At least the zero- and the 1<sup>st</sup> order beam have to be in the range of the aperture angle. If the incident light hits the mask under an angle  $\Theta_0 < \alpha$  the undiffracted beam enters the projection lens at the edge, and the 1<sup>st</sup> order beam is still collected by the lens, and therefore a pattern transfer is still possible. The angle of incidence  $\Theta_0$  can be realized by inserting an aperture in the optical path between condenser and mask (Figure 7b).

Although the higher resolution is an advantage of off-axis illumination, the impact on the depth of focus (DOF) is of even greater value. In on-axis illumination, the beams of different deflection orders have to travel in different ways so they are phase-shifted to each other, which results in a lack of focus. In off-axis illumination, the zero order and 1<sup>st</sup> order beam reaches the projection lens at the same distance from the center, which means that their optical path length is the same. So the relative phase difference between these beams is zero, which increases the DOF dramatically.

Off-axis illumination is facilitated by an aperture (Figure 8) which is located in front of the condenser lens. It depends on the apertures shape which structures are improved. If there is an aperture as in Figure 8a, only the structures perpendicular to the arrangement of the apertures will be improved. The aperture shown in Figure 8b yields an improvement of structures which are adjusted to good angles – up/down or left/right direction. This is sufficient because in normal cases, the features are in a good arrangement. The aperture in Figure 8c even decreases this problem, but here the improvement in DOF is less.

When the resolution in principle has to be improved, then according to the Rayleigh criterion either the wavelength  $\lambda$  or the technology parameter  $k_1$  have to be decreased, or the numerical aperture  $NA$  has to be increased.

Increasing  $NA$  means physically bigger lenses. Here the problem arises that it is difficult to produce huge lenses with the required quality; on the other hand the available materials also limit the physical size of the lenses. So there are still two possibilities of increasing the resolution: smaller  $\lambda$  and smaller  $k_1$ .

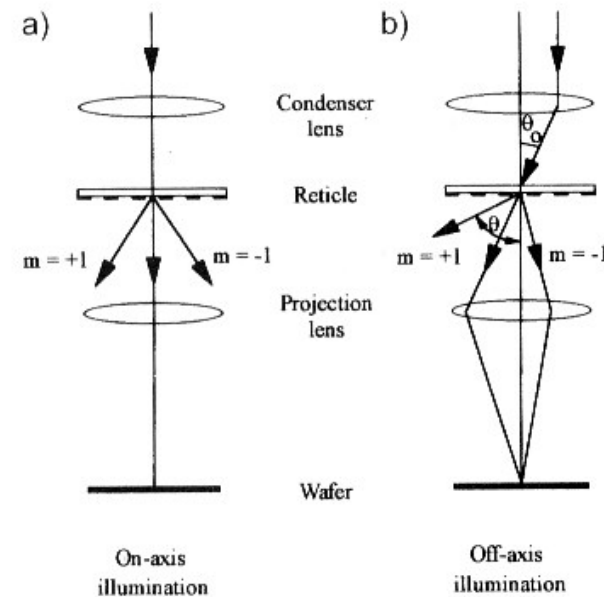


Figure 7:

(a) Optical path and deflection orders of on-axis and  
(b) off-axis illumination. Note that with the same wavelength and structure size, the off-axis illumination allows the 1<sup>st</sup> order beam to pass the optical system [3]. A good description of off-axis illumination is also found in [6].

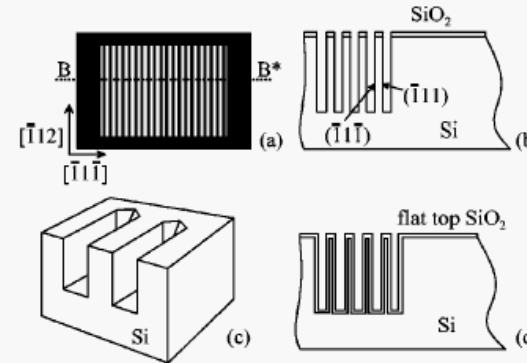
Da R. Waser Ed., Nanoelectronics and information technology (Wiley-VCH, 2003)

## Strategies to improve resolution III: anisotropic etching

An (110) silicon substrate ( $p$  doped, resistivity =  $1-10 \Omega \times \text{cm}$ ) was oxidized ( $1050^\circ\text{C}$  for 30 min) to obtain a 350 nm  $\text{SiO}_2$  layer. Standard photolithography was employed to pattern the oxide; the mask used is shown in Fig. 1(a). It consisted of an array of lines (width  $4 \mu\text{m}$ , length  $3000 \mu\text{m}$ , spacing  $4 \mu\text{m}$ ) which must be aligned along the  $[\bar{1}12]$  direction. After the oxide definition, an anisotropic etching was performed by means of an ethylenediamine-pyrocatechol (EDP) solution type F (fast) at  $115^\circ\text{C}$ .<sup>16</sup> After 1 h of etching walls with an high aspect ratio [Fig. 1(b)] (height= $35 \mu\text{m}$ , width in the range  $1-4 \mu\text{m}$ , depending on the alignment accuracy along the  $[\bar{1}12]$  direction) were obtained. For samples with a misalignment greater than  $0.07$  degrees there was a complete underetching of the planes.<sup>17</sup> Each array contained 1000 planes; Fig. 2 (top panel) shows a scanning electron microscope (SEM) micrograph of a cross section of an array of planes.

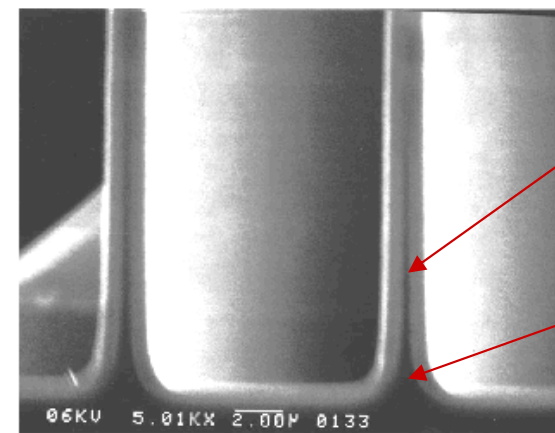
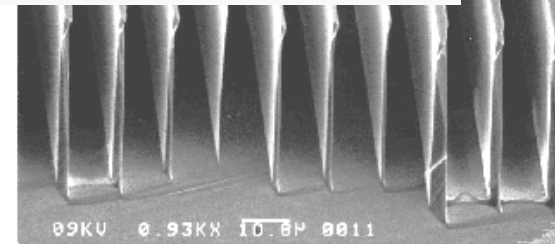
The samples were then etched in buffered HF (BHF) to remove the oxide mask layer indicated as  $\text{SiO}_2$  in Fig. 1(b), and underwent a oxidation. The sequence of oxidation/etching steps allowed to reduce the wall thickness in a controlled way, and PL measurements were carried out after each step to investigate the dependence of the emission features on the wall width. Figure 2 (bottom panel) is a closer view of a cross section of the planes, which shows that the Si core thickness is not uniform, an effect probably due to a minor oxygen diffusion at the bottom of the walls.

**Etching features can be used to improve the resolution**



Mask alignment

FIG. 1. Schematic view and orientation of the mask (a); result of the EDP etching (cross section along the line  $BB^*$ ) (b); a perspective view of the planes at the end of the etched zone (c); the two zones, flat top and array, where the PL was investigated (d).



Silicon oxide

Crystalline Silicon core

FIG. 2. SEM view of the array cross section (top panel); a closer view showing the oxidation effect (bottom panel).

# Strategies to improve resolution IV: side wall patterning

Processo di fabbricazione “complesso”  
(ma economico!!) per creare **Si-nanowires**:

a) ossidazione dry (spess.  $\leq 0.5 \mu\text{m}$ ):



seguita da deposizione  $\text{Si}_3\text{N}_4$  e patterning via **lito. ottica convenzionale**

b) CVD poly-Si (pirolisi  $\text{SiH}_4$  a bassa p):



c) Reactive Ion Etching del poly-Si con fascio ionico “inclinato”

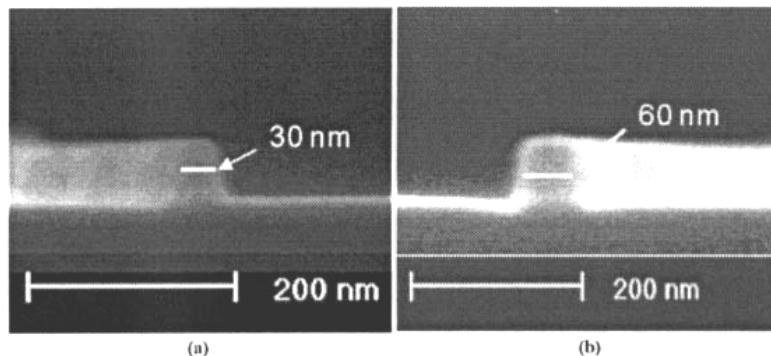
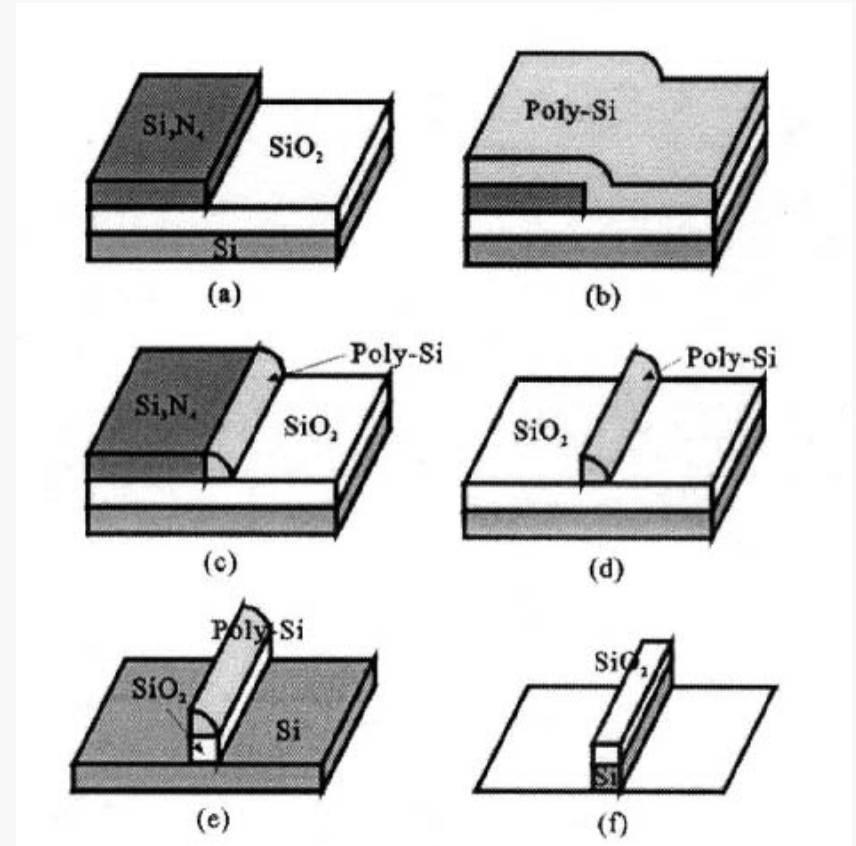
--> rimane poly-Si solo **sui bordi**

d) wet chemical etching **selettivo**

(soprattutto nitruro) con  $\text{H}_3\text{PO}_4$

e) rimozione ossido (poly-Si funge da maschera) con etching **selettivo**

f) rimozione nitruro con RIE non inclinata



SEM cross sections (in “prospettiva”)

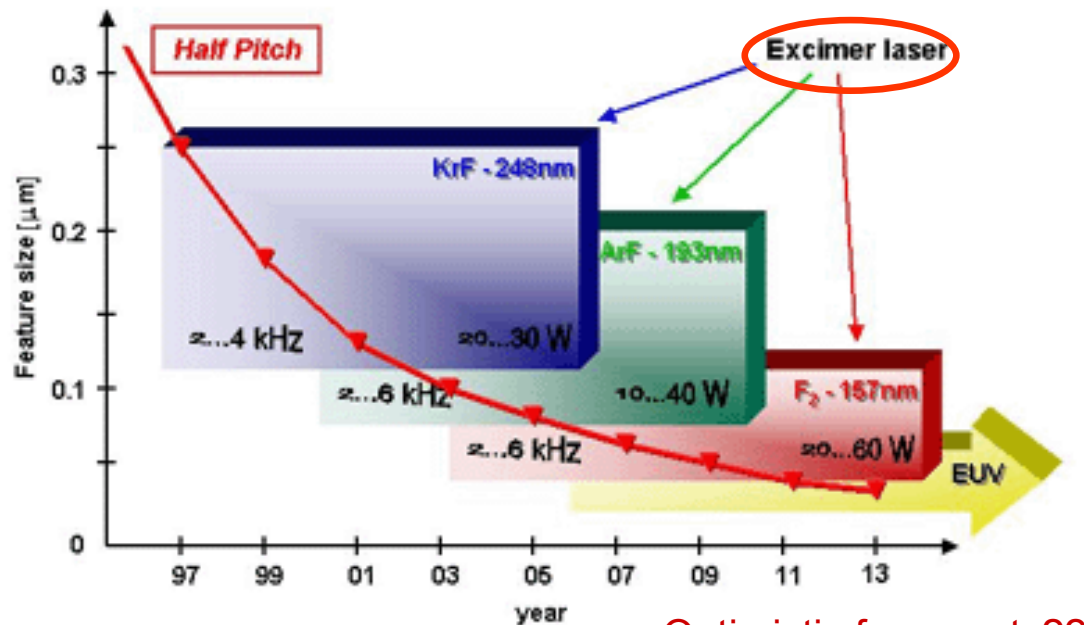
**Playing with etching process, results can be achieved comparable to electron beam lithography**

# Search for shorter (radiation) wavelengths

Rather obvious recipe to further improve space resolution: decrease the wavelength

Wavelength [nm]	Source	Range
436	Hg arc lamp	G-line
405	Hg arc lamp	H-line
365	Hg arc lamp	I-line
248	Hg/Xe arc lamp; KrF excimer laser	Deep UV (DUV)
193	ArF excimer laser	DUV
157	F <sub>2</sub> laser	Vacuum UV (VUV)
~10	Laser-produced plasma sources	Extreme UV (EUV)
~1	X-ray tube; synchrotron	X-ray

**Lambda Physik Lithography Roadmap**



Optimistic forecasts??

Continuous development of laser sources with smaller and smaller wavelengths (VUV)

# X-ray lithography (XRL)

XR source of choice: synchrotron

Brilliant XR beam

--> proximity mode masks

Resist: typ. PMMA

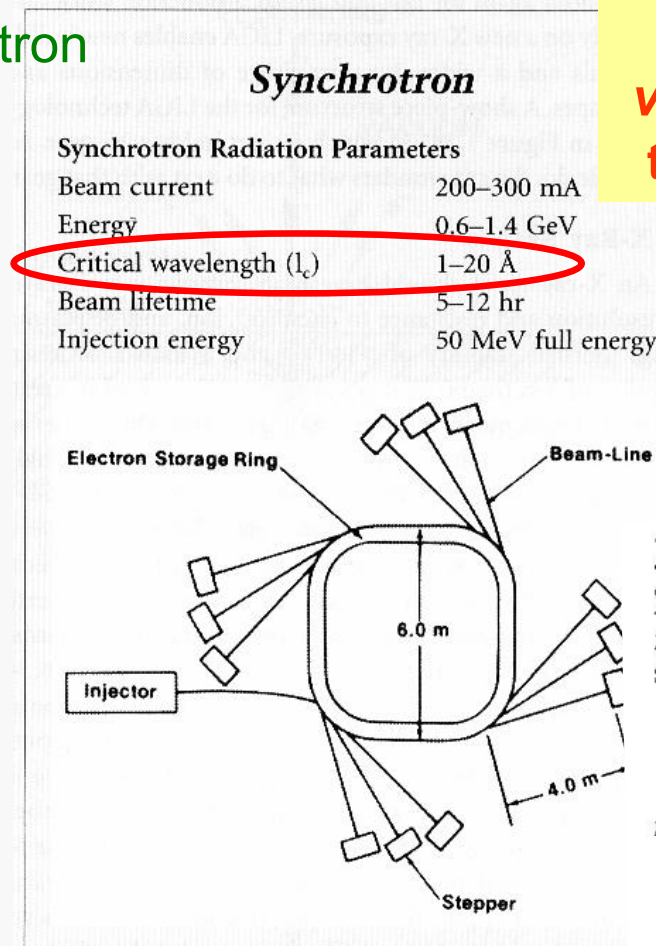
(critical sensitivity

--> large dose,  $\sim 2 \text{ J/cm}^2$ )

Masks:

Typ. Si membranes

**Diffraction problems  
virtually removed thanks to  
the very short wavelength**



Da M. Madou,  
Fundamentals of microfab.,  
CRC (1997)

TABLE 1.5 Optical vs. X-Ray Mask

Optical Mask	X-Ray Mask
Mask design: CAD	Mask design: CAD
Substrate preparation	Substrate preparation
Quartz	Thin membrane substrate (Si, Be, Ti, ...)
Thin metal film deposition	Deposit plating base (50 Å Cr, then 300 Å Au)
Pattern delineation	Pattern delineation
Coat substrate with resist	Coat with resist
Expose pattern (optical, e-beam)	Expose pattern (optical, e-beam)
Develop pattern etch Cr layer	Develop pattern
Strip resist	Absorber definition: Electroplate Au ( $\sim 15 \mu\text{m}$ for hard X-rays) Strip resist
Cost: \$1K–\$3K	Cost: \$4K–\$12K
Duration: 3 days	Duration: 10 days

**Effective resolution  $\sim$  tens of nm  
Large depth of field -> suitable for high  
aspect-ratio features, micromachining, ...**

## 4 X-Ray Lithography

Decreasing the wavelength even further into the x-ray range yields so-called x-ray lithography. For these short wavelengths it is not possible to set up an optical path neither in reflection optics nor in refraction optics. On one hand, there is no material which is transparent enough to make lenses or masks from, and, on the other hand, it is not possible to make Bragg-reflectors. The individual layers in the layer stack have to have a thickness of  $\lambda/4$ , which corresponds to a layer thickness of  $\sim 0.3$  nm. This is in the range of the thickness of one monolayer and is not achievable..

Projection x-ray-lithography is therefore not possible, but proximity x-ray lithography (PXL) is possible. The advantages are the high resolution limit ( $\sim \sqrt{\lambda \cdot (g+d)}$ , which is about 30 nm for 1 nm exposure wavelength) and the insensitivity to organic contamination. These contaminations (as all low atomic number materials) do not absorb the x-rays, and hence are not printed onto the sample.

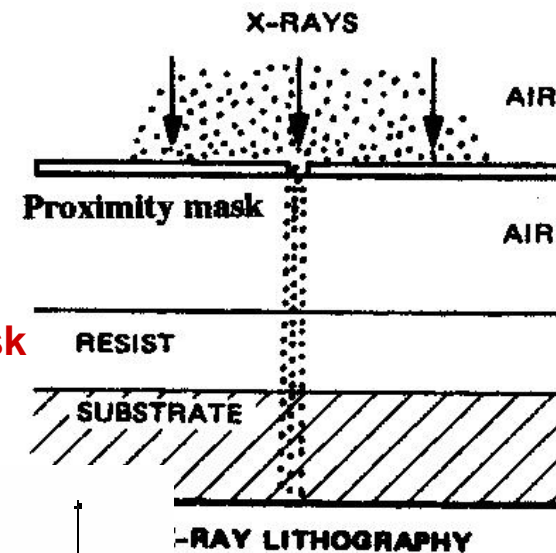
But there are some limitations. Consider a source with diameter  $a$  of 1 mm at distance  $L$  of 1 m towards the mask and a proximity gap  $g$  of 10  $\mu\text{m}$ . Then there is the so-called penumbral blur  $\xi = a \cdot g / L \sim 10$  nm, which limits the resolution (Figure 16). Furthermore, the pattern is not transferred correctly to the sample. Even if a point source is used, there is a displacement  $\Delta$  of  $\Delta = r \cdot g / L$ , where  $r$  is the radial position on the sample (Figure 16). This error can be eliminated if it is taken into account when the mask pattern is generated.

Nevertheless, if synchrotron radiation is used, a high intense beam of parallel light is available so these errors do not occur. This parallel beam has another advantage: Due to the small deflection the exposure shows a high depth of focus of several  $\mu\text{m}$ , facilitating exposures of textured substrates or of thick resists (Figure 17).

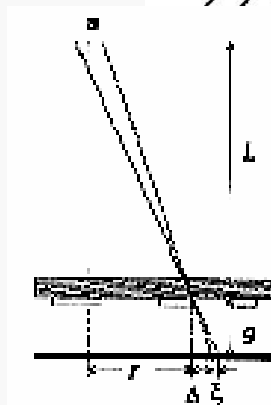
The problem for PXL is the masks. Since there is no material which is as transparent to x-ray as quartz to DUV, the carrier layer has to be thin (1 – 2  $\mu\text{m}$ ). On the other hand, there is also no material which is as opaque to x-ray as chromium to DUV, so the masking layer has to be thick enough (300 – 500 nm). A carrier layer of 1  $\mu\text{m}$  SiC only has a transparency of 57 %, while a masking layer of Au still lets 14 % of the light pass. The absorbed light will heat the mask so that it expands, which leads to another uncertainty in the pattern transfer. Furthermore, PXL is a non-reduction printing method, so the features on the mask are of the same size as on the sample. This makes the production of the masks very complicated when the target is the sub-100 nm range.

The mask production sequence is as follows: On a silicon wafer, a thin membrane layer is deposited (e.g. SiC, Si<sub>3</sub>N<sub>4</sub>). Onto this layer, a chromium etch stop layer and the masking layer of 300 – 500 nm of a high-atomic number material is evaporated (e.g. Au Ta). Then the mask is coated with an e-beam resist and exposed in an e-beam direct-write system. The resist is used to etch the masking layer with an etch stop on the chromium so the membrane is not hurt.

The commonly used DUV resists show good process aptitude.



Proximity mask



Mask materials

Penumbral blur

Figure 16a Penumbral blur  $\xi$  and displacement error  $\Delta$  for proximity x-ray lithography.  $L$  is the distance from source to mask,  $g$  is the proximity gap and  $a$  is the lateral diameter of the source [1].

Large scattering of secondary electrons limits the resolution

# 4. Use of charged particle beams

## Matter waves instead of radiation

Basic components:

- electron optics;
- accelerated particles

First “peculiarities” of the implementation:

- large kinetic energy (tens of KeV) --> possible sample damages
- care required to fix the electric potential  
→ typ. applied to conductive substrates
- need for UHV environment
- inherently **serial (scanning) technique**

### 4.1.1 Wave Properties of Electrons

The focusing of an electron beam is possible because of the dual, *wave-particle* character of electrons. This wave-particle duality is expressed in the *de Broglie relationship* for the wavelength of a particle:

$$\lambda = h/mv \quad (4.1)$$

where  $m$  is the mass of the particle,  $v$  is its velocity and  $h$  is the Planck constant. Assuming that the accelerating voltage in the electron gun is  $V$ , then the electron energy is given by:

$$mv^2/2 = eV \quad (4.2)$$

where  $e$  is the charge on the electron. It follows that  $\lambda = h/(2meV)^{0.5}$ , or  $\lambda = (1.5/V)^{0.5}$  nm when  $V$  is in volts. This numerical value is approximate, since at the accelerating voltages commonly used in the electron microscope, the *rest mass* of the electron,  $m_0$ , is appreciably less than the *relativistic mass*,  $m$ , and a correction term should be included, in the equation:

$$\lambda = \frac{h}{\sqrt{2m_0eV \left(1 + \frac{eV}{2m_0c^2}\right)}} \quad (4.3)$$

where  $c$  is the velocity of light. The relativistic correction amounts to *ca* 5% at 100 kV, rising to 30% at 1 MV. The electron wavelength at 100 kV is 0.00370 nm, which is nearly two orders of magnitude less than the interatomic spacings typical of the solid state. At 10 keV, which is typical of many applications of scanning electron microscopy, the wavelength is only 0.012 nm, still appreciably less than the interatomic distances in solids.

**De Broglie wavelength is much smaller than radiation wavelength  
→ diffraction has negligible effects**

# Electron microscopy

As in optical methods, also with electrons microscopy and lithography are two faces of the same topic

Before discussing electron lithography, **electron microscopy** must be introduced

As in optical microscopy, both “reflection” and “transmission” of the electron beam from the sample can be acquired, leading to **SEM** and **TEM**, respectively

In case of TEM, sample must be thinned in order to be “semi-transparent”

**Figure 16:** Schematic procedure to prepare a planar sample for TEM. After preparing the sample on an substrate the latter may be etched. The final thickness of some 100 nm can be achieved by ion milling. The up pointing arrows denote the direction of the TEM beam.



(...a complicated and destructive procedure!!)

Electron microscopy relies on some **contrast mechanisms**, i.e., mechanisms ruling the behavior of transmitted or scattered (in case of TEM or SEM) electrons as a function of the local sample properties

# A few words on contrast mechanisms in TEM

In TEM elastic interaction is predominant; main contrast mechanisms are:

1. **mass thickness** (transmission depends on the amount of mass crossed by the electrons)
2. **diffraction** (in crystalline materials Bragg diffraction plays a role leading to high sensitivity to lattice defects)
3. **phase contrast** (when collection optics has a large numerical aperture, due to mutual interference of many diffracted beams)

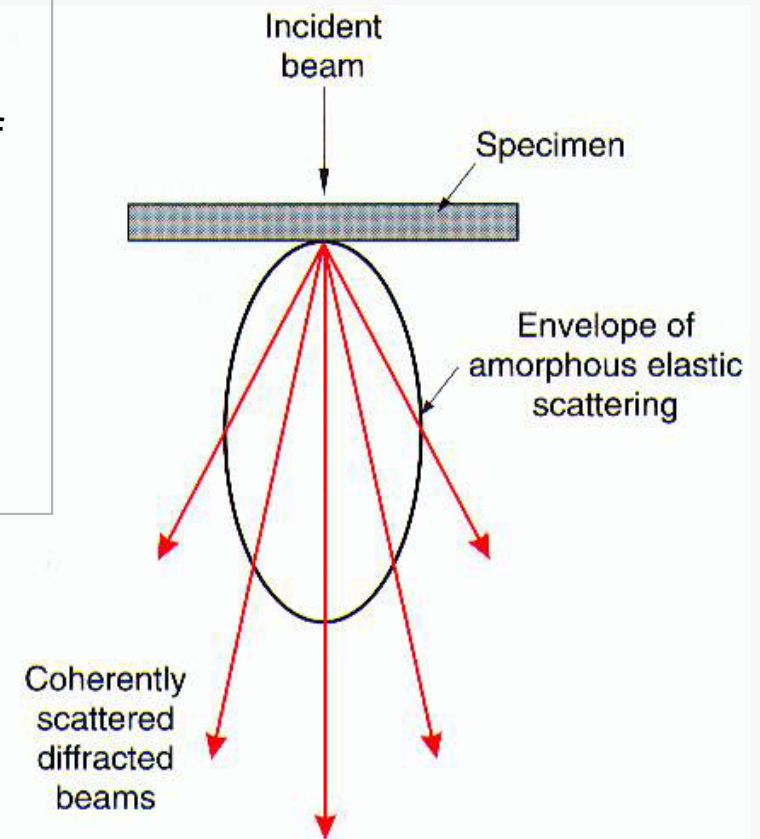


**Figure 4.12** The incident beam is elastically scattered by the sample, either randomly (a lassy or amorphous specimen), or coherently (a crystalline phase). The image may be formed from the direct transmitted beam, by a diffracted beam, or by the interference of the diffracted beams with each other and/or the direct transmitted beam (see text for details)

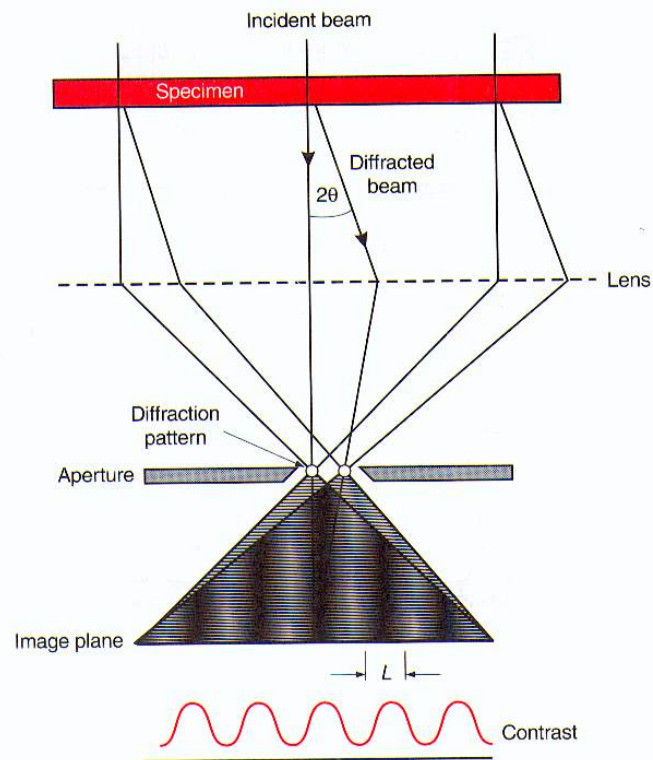


**Figure 4.15** If the objective aperture accepts a Bragg-diffracted beam as well as the direct transmitted beam,  $\alpha > 2\theta$ , then an interference pattern will be formed in the image plane as a result of the difference in path lengths of the two beams

**Morphological and topographical information are somehow “convoluted”, but space resolution is excellent**

# Secondary electron generation (SEM)

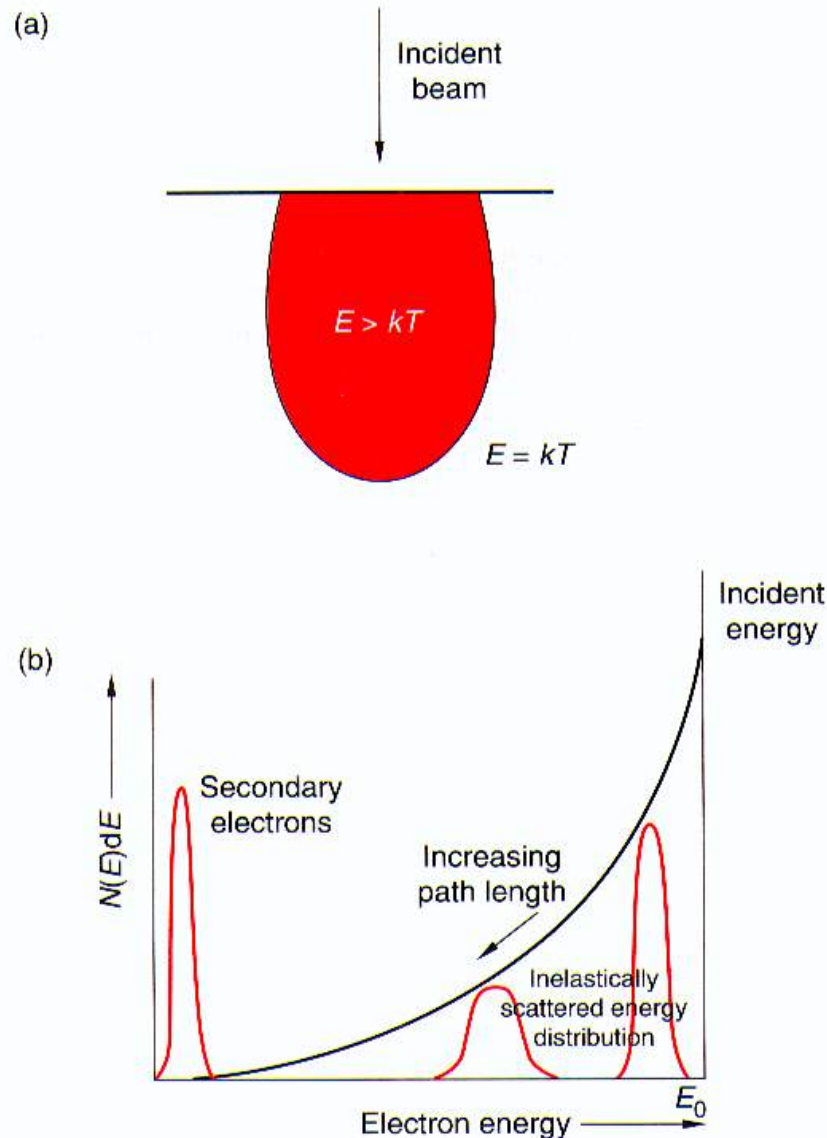


**Figure 4.29** (a) The electron beam is inelastically scattered within an envelope bounded by the condition that the average energy has reached the thermal kinetic value  $kT$ . (b) The energy spread increases and the average energy of the electron falls as the path length within the solid increases (channelling effects and lattice anisotropy being ignored). (c) Random scattering models for individual electrons (Monte Carlo simulation) provide a vivid image of both the energy distribution and the spatial distribution of the electrons in the volume of the material beneath the beam, as well as the origin of the back-scattered electron signal

SEM does not require sample to be crossed by electrons:

- **Thick films** can be analyzed
- Strong dependence on conductivity (dielectric samples must be **metallized**)
- **Secondary electrons** are produced (inelastic scattering)
- **Space resolution is lower than in TEM** (contrast is based on less sensitive processes)

**In SEM inelastic scattering is predominant**

## A few words on contrast mechanisms in SEM

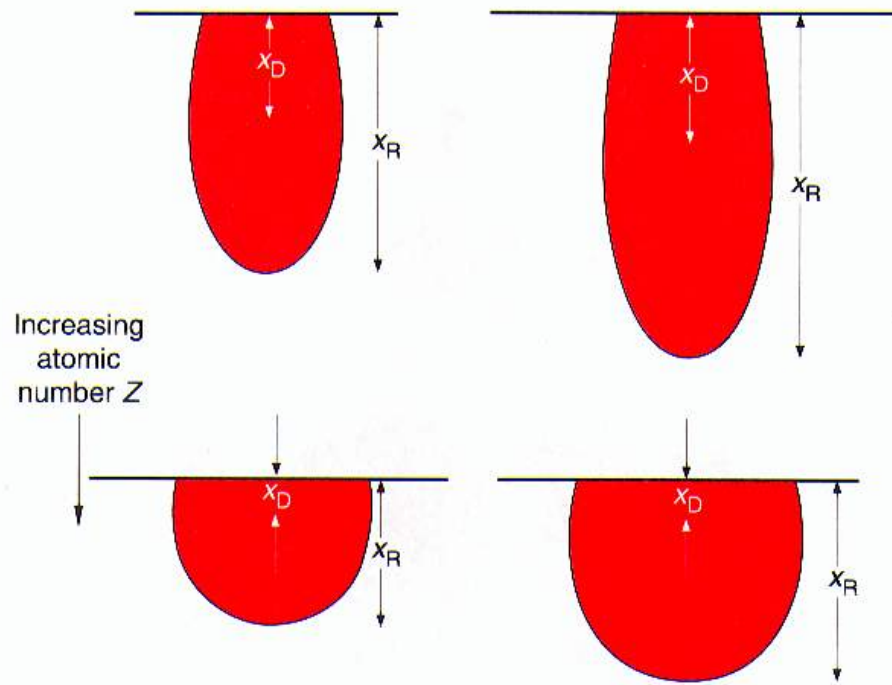
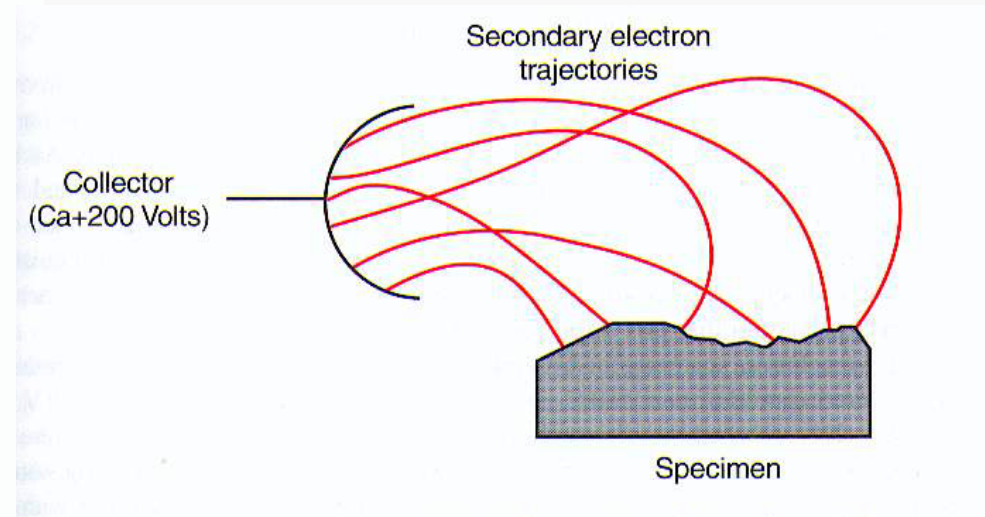


**Figure 4.30** The inelastic scattering envelope for an incident beam of energetic electrons depends on both the incident energy and the atomic number of the target, and is qualitatively characterized by the two parameters, diffusion depth, and penetration depth (or range)



**Space resolution associated to the size of the electron focal spot, not to the collection of secondary electrons**

Scattering cross sections depend on the atom number  $Z$   
Energy of the secondary electrons depend on the electronic configuration  
Secondary electron yield depends on penetration length, i.e., on the material properties

**Microanalysis** methods can be implemented in SEM  
(e.g.: X-ray Photoelectron Spectr. - XPS, Rutherford BackScattering - RBS, Secondary Ioniz. Mass Spectr. - SIMS, ...)

# Scanning Electron Microscope (SEM)

Typ. Filament source (ddp 10-100 kV):

W:  $j \sim 5 \times 10^4 \text{ A/m}^2$

LaB<sub>6</sub>:  $j \sim 1 \times 10^6 \text{ A/m}^2$

field emitter:  $j \sim 5 \times 10^{10} \text{ A/m}^2$

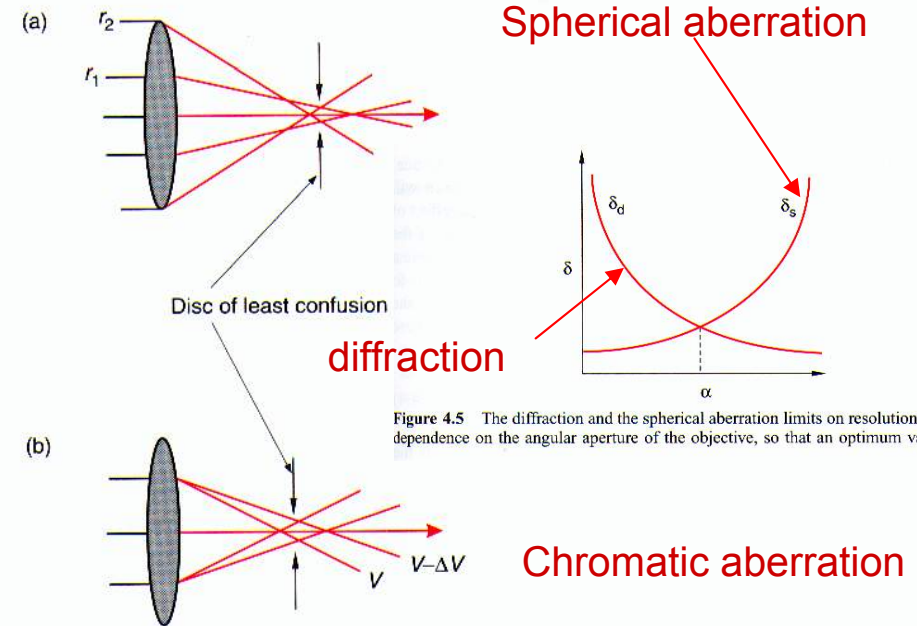
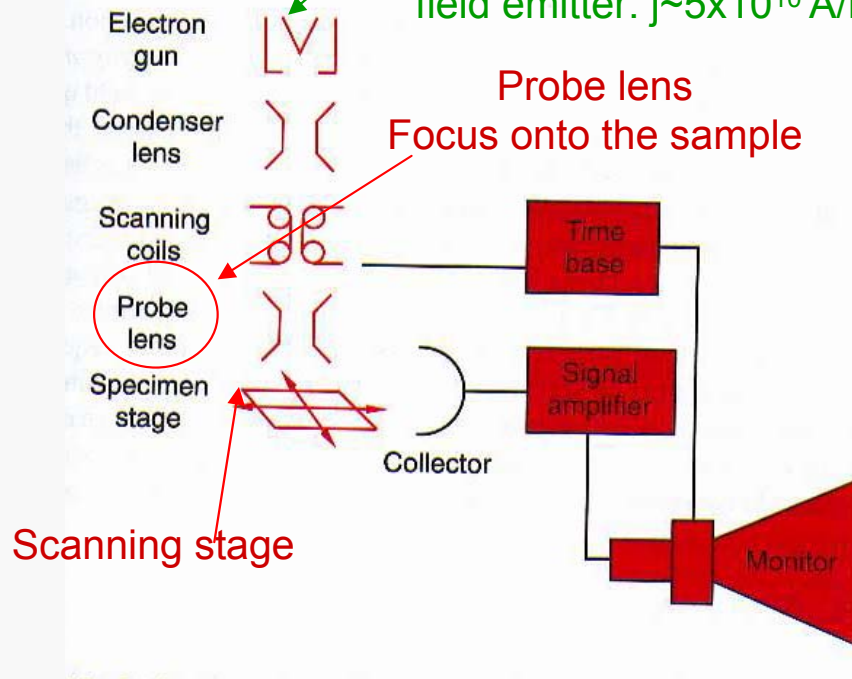


Figure 4.5 The diffraction and the spherical aberration limits on resolution have an opposite dependence on the angular aperture of the objective, so that an optimum value of  $\alpha$  exists

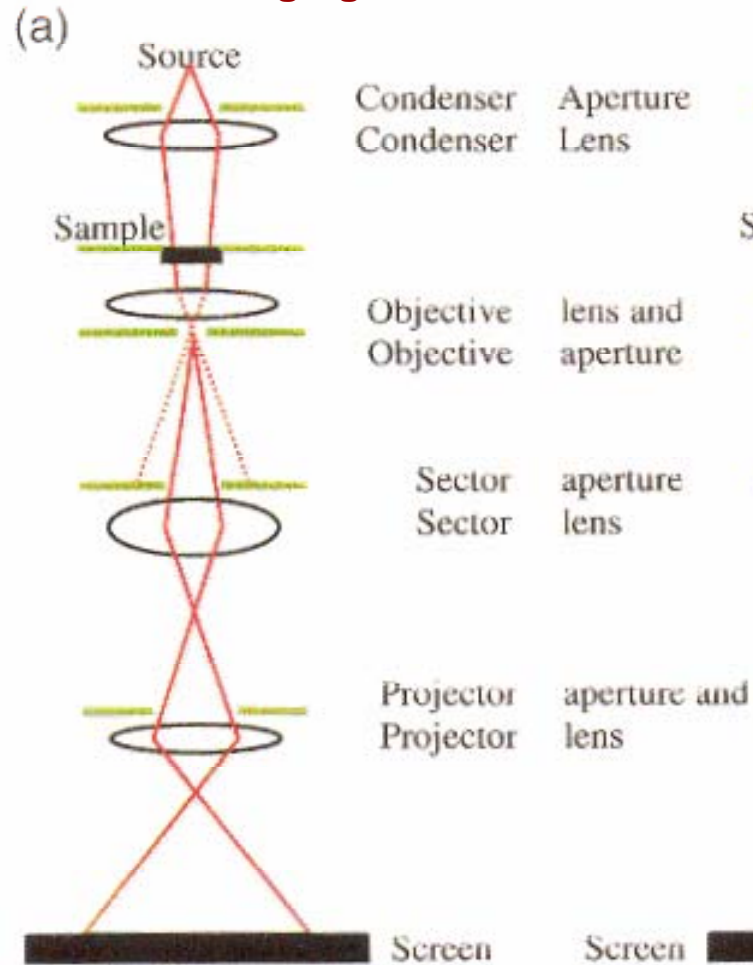
Figure 4.4 Spherical (a) and chromatic aberration (b) prevent a parallel beam from being brought to a point focus. Instead, a disc of least confusion is formed in the focal plane

Scanning Electron Microscope (SEM)  
relates to electron beam lithography  
as  
Optical Microscope  
relates to optical lithography

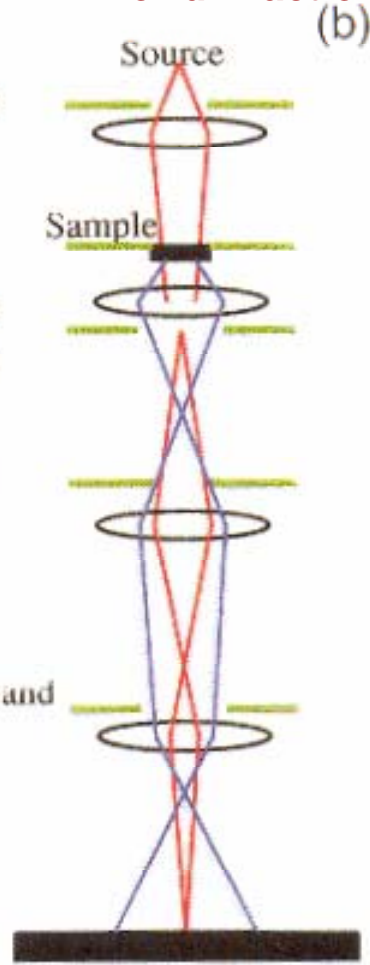
Electron optics similar to  
conventional optics in terms  
of problems and strategies

# Transmission Electron Microscope (TEM)

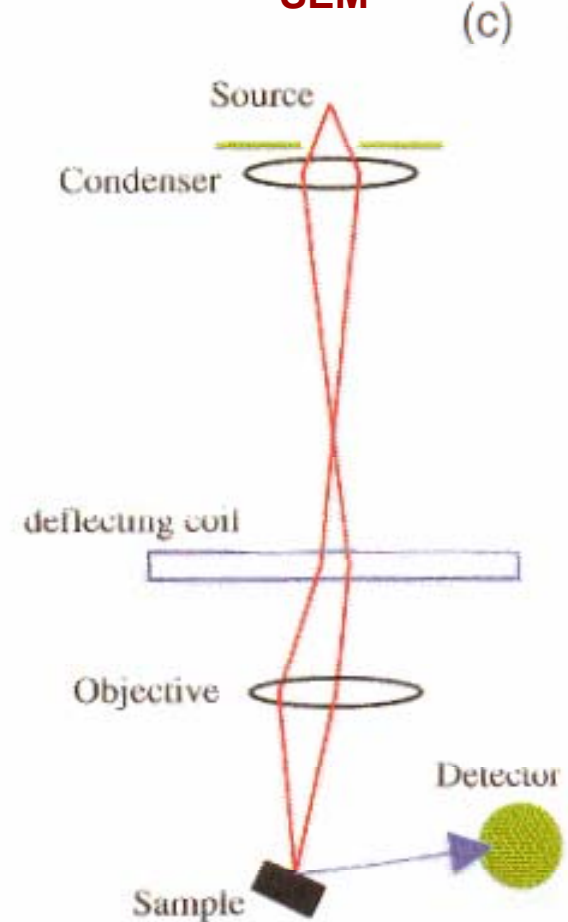
## TEM for imaging



## TEM for diffraction



## SEM



Diffraction TEM can be achieved by simply modifying the numerical aperture of the collecting electron optics (**bright and dark field images**)

**Note the need for UHV environment and the serial (scanning) nature!**

## Examples of high resolution TEM

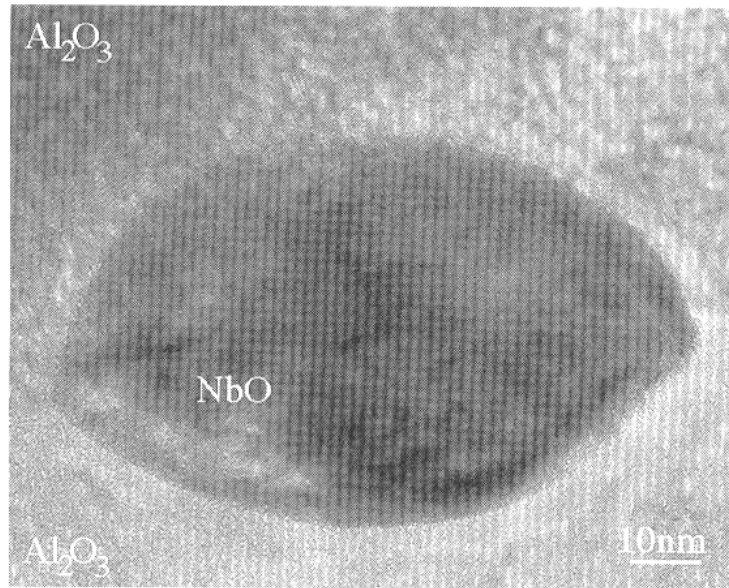


Figure 4.53 Transmission electron micrograph of a NbO particle located at a grain boundary in polycrystalline alumina. Phase contrast (lattice fringes) and mass-thickness contrast vary from the alumina grain to the NbO grain

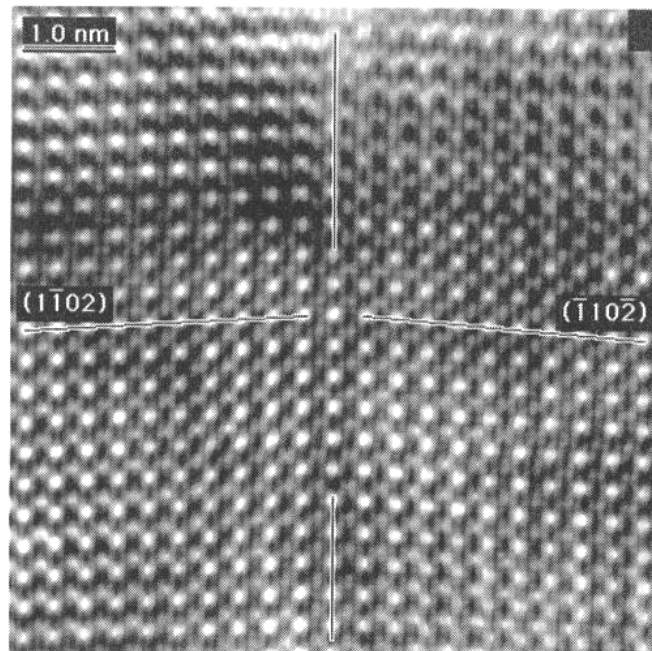


Figure 4.54 Lattice image of a rhombohedral twin in alumina

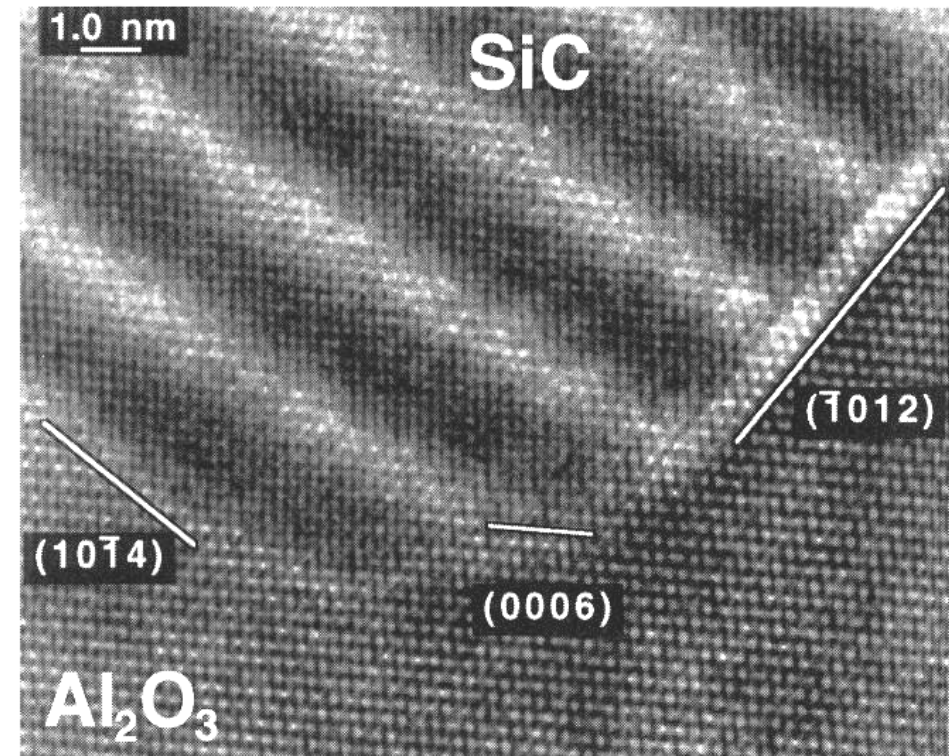


Figure 4.55 Lattice image of a SiC particle located within an alumina grain. The alumina lies along a low-index-zone axis, and is the source of the lattice image. A moiré pattern appears within the SiC particle due to overlap between the alumina and SiC (in the direction of the electron beam)

**Atomic resolution achieved along with structural information**

# 5. Writing patterns with electron beams

## 5.1 Electron Beam Direct Write

In electron beam direct write electrons are formed to a beam and are accelerated to a determined position on the wafer surface, where the resist has to be exposed to form the pattern. An electron beam system consists of the electron source or electron gun, the electron-optical system (the electron column), a mechanical wafer stage and a controller system. A schematic view of an electron beam lithography tool is given in Figure 18.

The two types of electron guns which are commonly used are thermionic sources, on the one hand, and field emission sources, on the other hand. In thermionic sources the electrons are emitted by heating the source material, such as tungsten (W) or lanthanum hexaboride (LaB<sub>6</sub>). While LaB<sub>6</sub> offers a higher brightness ( $10^5$  (A/cm<sup>2</sup>)/steradian) and a longer lifetime (~1000 h) than W ( $10^4$  (A/cm<sup>2</sup>)/steradian; ~100 h), W has the advantage that vacuum requirements are not as high as for LaB<sub>6</sub>. Nevertheless, LaB<sub>6</sub> has become the standard source for thermionic e-beam sources.

In field emission sources the electrons are extracted from a sharp tip by a high electric field. Though these sources have a high brightness ( $10^7$  (A/cm<sup>2</sup>)/steradian), they are unstable and require a ultrahigh vacuum. Therefore they have not been widely adopted in electron beam lithography systems.

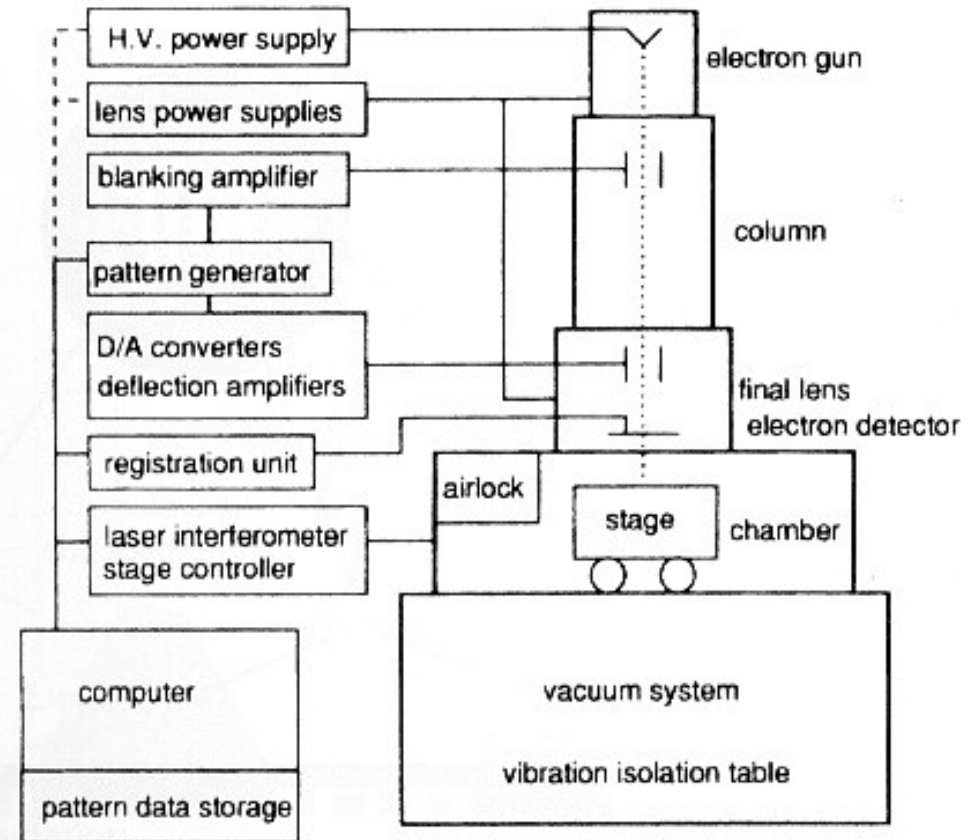
In the electron column the extracted electrons are formed to a beam with a definite diameter or shape. Therefore different electron-optical elements as focusing and defocusing lenses and apertures are employed. Further parts of the column are a beam blank to switch the beam on and off and a beam deflection system, with which the beam is positioned on the wafer.

Since the deflection system can only address a field of 400 – 800 μm (depending on spot size and tool), it is necessary to move the sample under the beam from one exposure field to the next by a mechanical wafer stage. The position of the stage is measured by an interferometer, so it is possible to adjust the beam with an accuracy of ~5 nm.

The whole system has to be under vacuum to enable the electron beam to be formed and has to be isolated from vibrations. Further requirements are low electromagnetic stray field, because this would hamper the positioning of the beam.

The pattern, which is given as a CAD file, is translated into movements of the electron beam/wafer stage by a computer. During an illumination, the tilt of the sample is measured continuously and the focus is adjusted. There are two exposure schemes: In the first one, the raster scan scheme, the deflection system and the wafer stage address every point of the sample, but the beam is switched on and off according to the structure. In the second scheme, the vector scan scheme, only the points which have to be illuminated are addressed. Hence the vector scan scheme is less time-consuming than the raster scan scheme.

The time needed for the illumination of a whole wafer depends on the pattern, but because the electron beam direct write is a serial method, it is time-consuming and not suitable for the industrial mass production of microelectronic circuits. Nevertheless, because the resolution is pushed to a few nanometers, it has a high impact on research activities and is the method of choice for defining the pattern on the masks used for optical lithography.



**The electron beam of a SEM can be used to “write” an arbitrary pattern onto a surface**

# Electron Beam Lithography (EBL)

Accelerated charged particles can be used for:

- etching, milling etc. (better with heavy ions, see FIB)
- **resist impression** (*true* electron beam lithography)

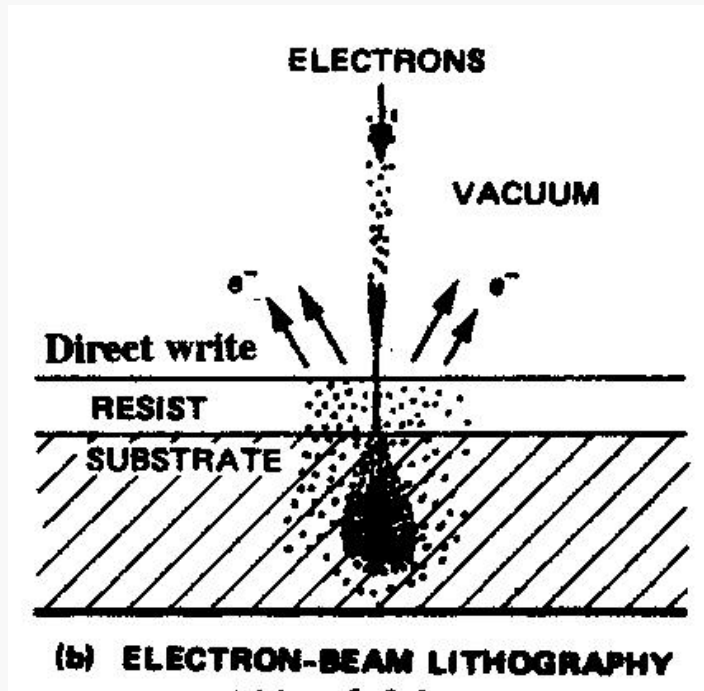


TABLE 1.6 Electron- and Ion-Beam Applications

Electron-Beam Applications	Ion-Beam Applications
Nanoscale lithography	Micromachining and ion milling
Low-voltage scanning electron microscopy	Microdeposition of metals
Critical dimension measurements	Maskless ion implantation
Electron-beam-induced metal deposition	Microstructure failure analysis
Reflection high-energy electron diffraction (RHEED)	Secondary ion mass spectroscopy
Scanning auger microscopy	

Da Madou,  
Fundamentals  
of microfabr.  
CRC (1997)

**Excellent space resolution (similar to SEM/TEM, i.e., below 10 nm)  
but serial and complicated process, unsuitable for large-scale applications**

# Electron beams for EBL

Actual space resolution associated to beam **focusing**

Intense beams are required, but excess kinetic energy (ddp) should be avoided  
→ **field emitters** (eventually, in arrays to mimic parallel writing)

## *Field and thermionic emission and photoemission*

(From Lindquist et al., *Research and Development*, June, 91–98, 1990. With permission.)

### Electron emission in a water bucket

THE THREE MECHANISMS used by field emission sources all basically involve emitting electrons and ions from a metal surface under the influence of a strong electric field.

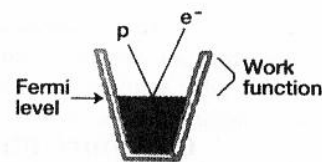
Understanding these mechanisms is where the water bucket comes in.

In this analogy, the water level in a bucket represents the Fermi level—the highest occupied energy level in a cathode material. The work function is the energy required to get the water droplets (electrons) from the top of the liquid out of the bucket. This is the distance equivalent to the potential energy barrier.

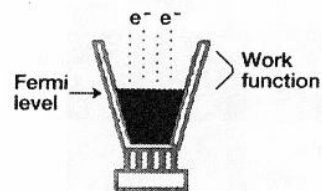
In photoemission, photon energy excites electrons at the Fermi level of the cathode material and can impart enough kinetic energy to allow the electrons to escape from the bucket.

In thermionic emission, heat thermally excites the electrons, providing enough energy to boil the electrons off and out of the bucket.

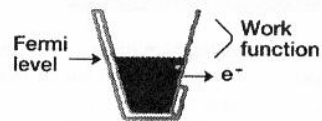
In field emission a high electric field can thin the side of the bucket enough so that the electrons can tunnel through it.



Photoemission

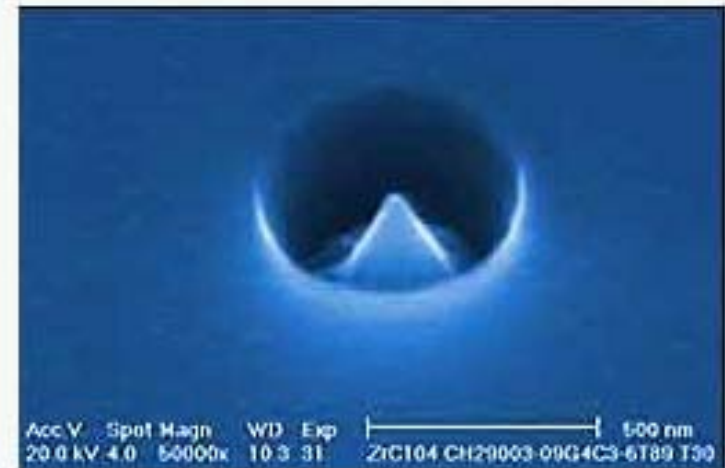


Thermionic emission



Field emission

## Micro- and nano-fabricated field emitters



This carbide crystalline tip, with a radius of 100 angstroms, or 10 nanometers at the top and 0.5 micron at the base, emits electrons in a tiny beam.

**Cumbersome preparation and manipulation of charged-particle beams (e.g., Coulomb self-repulsion)**

# Resists for EBL

Organics or inorganics thin films (e.g., fluorides, amorphous chalcogenides, AsS, AsSe,...)

**Technological problem of EBL:**  
Inelastic scattering of particles



- Robust and compact resists needed
- Very thin resist layers to prevent inelastic scattering
- Extremely careful control of the dose

**Space resolution strongly affected by the resist properties**

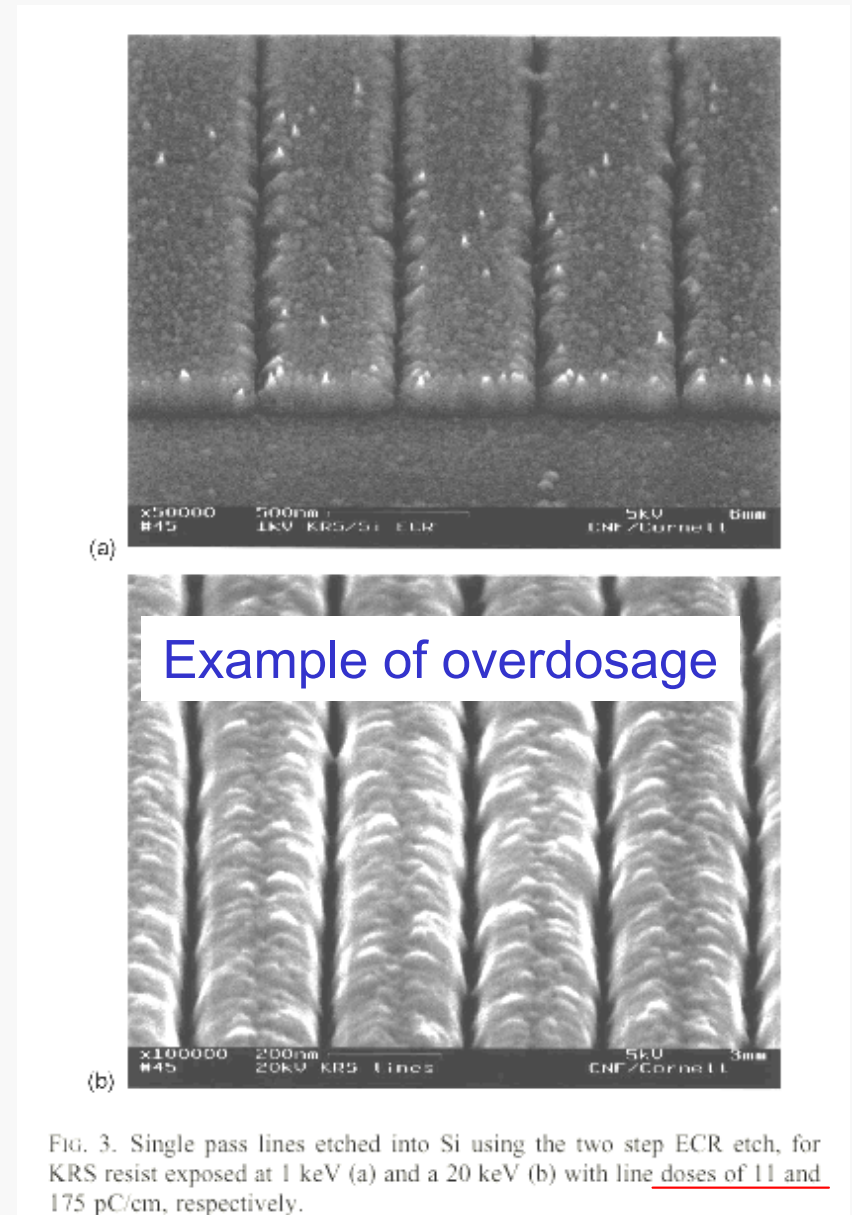


FIG. 3. Single pass lines etched into Si using the two step ECR etch, for KRS resist exposed at 1 keV (a) and a 20 keV (b) with line doses of 11 and 175 pC/cm, respectively.

# The SCALPEL technique

## 5.2 SCALPEL

The drawback of electron beam direct write is the serial character of the method. In mass production, where throughput is concerned, exposure times of several hours are not acceptable. Though there are electron optics which could enable projection lithography analogously to optical projection lithography, this method suffers from the huge penetration depth of electrons. The masking layers have to be thick to stop a significant part of the electrons.

One method of circumventing this problem is the SCALPEL method (scattering with angular limitation in projection electron beam lithography). In SCALPEL a broad beam of electrons, 2 to 3 mm in diameter, is scanned across a mask consisting of a silicon-nitride membrane layer (~100 – 150 nm), on which a patterned scattering layer (25 to 50 nm of gold or tungsten) is situated (Figure 20a). The electrons, which only strike the membrane layer, will pass this layer mostly unscattered, while the electrons, which strike the scattering layer, will be distracted strongly from their path. The unscattered electrons are focused through an aperture and projected onto the wafer, while the scattered electrons will be blocked. So a high contrast image can be achieved.

As a projection lithography method, SCALPEL offers the advantage of image reduction thus making mask fabrication easier. The mask itself consists of silicon struts, between which the membrane layer is clamped (Figure 20b). The width of the membrane corresponds to the diameter of the electron beam, while it is a few cm in length. By means of the projection optics behind the aperture the electrons coming from two different membrane areas separated by a silicon strut can be stitched together at the wafer, so circuits of 2 cm times 3 cm can be exposed.

Attempts to overcome the limitations of a scanning technique with a “beam projection” approach

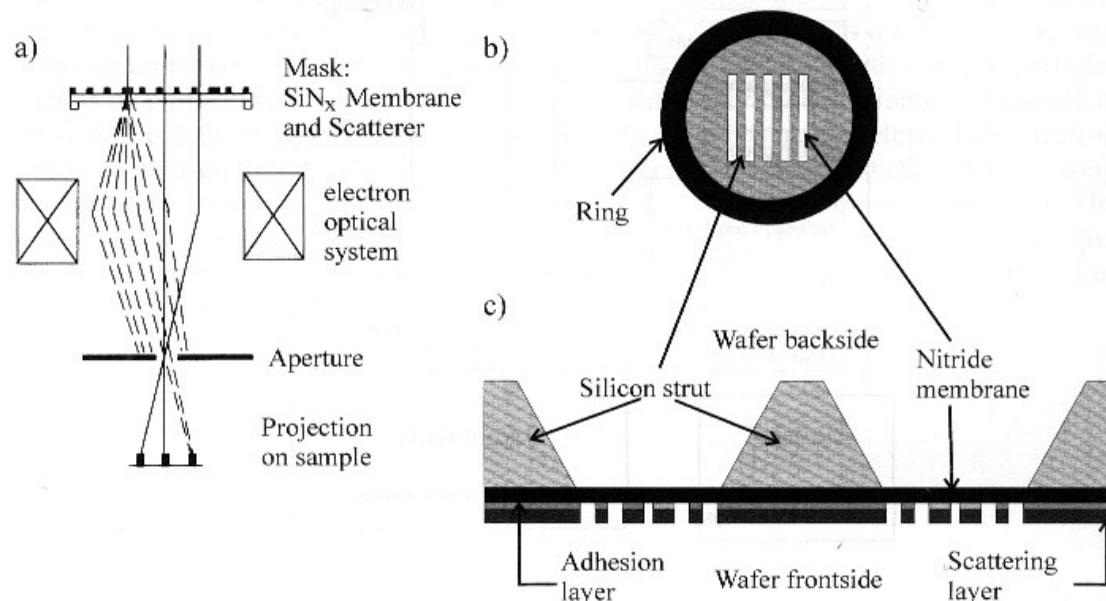


**Figure 20:**

(a) Electron path through a SCALPEL tool. A parallel beam of electrons passes through the mask; a scattering layer in which the pattern is inscribed scatters the electrons, so that they are not focused through an aperture by the electron optical system; only the unscattered electrons will pass the aperture. These electrons are projected onto the sample [16], [43].  
(b) Top view of a mask and  
(c) cross-sectional view of the mask. The masks are strips and separated by silicon struts. The masks are illuminated in series and the pictures of the masks are projected onto the adjacent sample.

# Focused Ion Beam (FIB)

## 6.1 Focused Ion Beam

The setup of a focused ion beam (FIB) tool is similar to an electron beam lithography tool, but instead of an electron beam a focused ion beam is used either to expose a resist locally, as in electron beam lithography, or to modify the substrate directly. The heavy ions impinging on the surface will sputter the material or, depending on energy, will intermix the layers at the surface of the sample. By means of this so-called ion milling the properties of the material at the surface will be altered. Another possibility is the local deposition of an additional layer. The impinging ions can induce the decomposition of a gas. As in a Chemical Vapor Deposition (CVD) process, where the decomposition of the process gases is induced globally by thermal activation (Low Pressure CVD) or by a plasma (Plasma Enhanced CVD), this local decomposition leads to a local deposition of the material.

Besides a certain impact on the structure definition in the research environment, the direct modification of the surface, the sputtering as well as the deposition, enables the method to be used in the most important application of FIB in industry, namely mask repair. Mask production is very expensive and due to some failure in the processing (e.g. dirt sticking on the mask or a mistake in the electron beam pattern generator) a mask can be faulty. Either some parts of the masking layer, which should have been removed, are still present, or some parts of the masking layer are removed in excess. These faults can be cured by FIB.

**Focused ion beams (accelerated) can be used as well (typ., for nanomachining)**

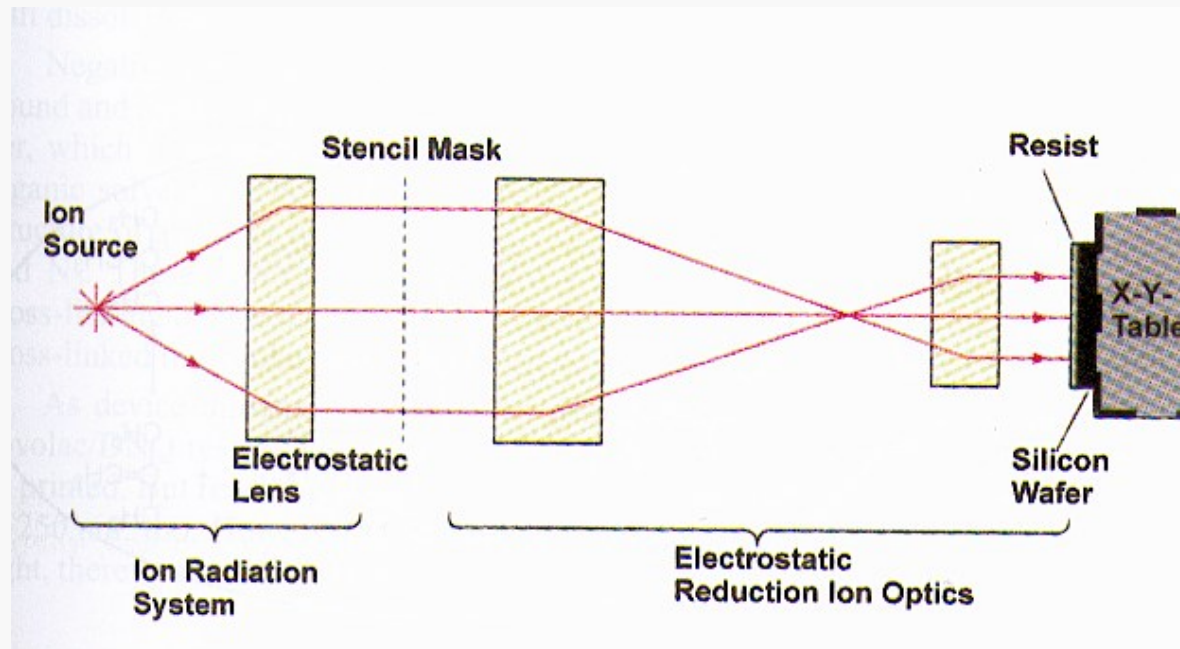


**Figure 21:** Schematic view of an ion projection lithography tool.

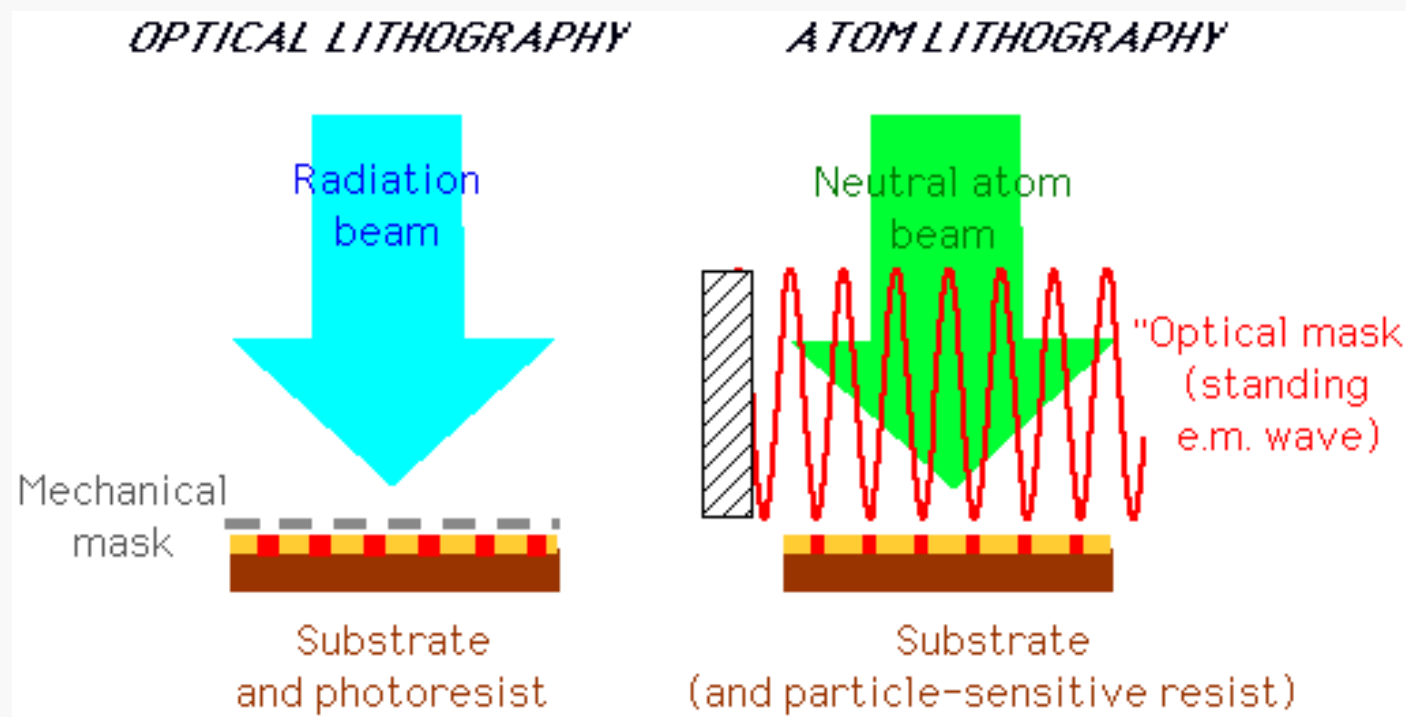
## 6. Alternative approaches based on atom optics

Basic idea: use of a **neutral** particle beam

--> sub-nm ( $\lambda_{dB}$ ) diffraction *without the problems of electron optics*

Further potential advantages:

- use of “optical masks” (non obtrusive, species-selective, defect-free...)
- possibility of direct deposition (**bottoms-up at the atom level**) or resist-assisted
- parallel character like optical lithography



**Main ingredient:  
Atom optics, i.e., laser manipulation (cooling) of neutral atoms**

## A few words on atom optics

**Optical mask** (standing e.m. wave)

--> **dipolar forces** (conservative)

Along a direction transverse to atom beam

Meschede Metcalf  
JPD (2003)

The optical dipole force acting on an atom with resonance frequency  $\omega_A$  in a laser field of detuning  $\delta = \omega_L - \omega_A$  is derived from the spatial variation of the light shift  $\omega_{ls}(r)$  [1]. For a single laser beam travelling in the x-direction with Rabi frequency  $\Omega$ , the light shift is given by

$$\omega_{ls} = [\sqrt{\Omega^2 + \delta^2} - \delta] / 2. \quad (1)$$

For sufficiently large detuning  $\delta \gg \Omega$ , approximation of Eq. 1 leads to  $\omega_{ls} \approx \Omega^2 / 4\delta = \gamma^2 s / 8\delta$ , where  $s \equiv I / I_{sat}$ ,  $I$  is the laser beam intensity,  $I_{sat} \equiv \pi \hbar c / 3 \lambda^3 \tau$  is the saturation intensity, and  $\tau \equiv 1 / \gamma$  is the atomic excited state lifetime.

In a standing wave with  $\delta \gg \Omega$ ,  $\omega_{ls} = \omega_{ls}(x)$  varies sinusoidally from node to antinode and also spontaneous emission is inhibited so that  $\hbar \omega_{ls}(x)$  may be treated as a potential  $U(x)$ . The resulting dipole force is

$$\mathbf{F}(x) = -\nabla U(x) = -\frac{\hbar \gamma^2}{8\delta I_{sat}} \nabla I(x) \equiv U_{max} \nabla f(x), \quad (2)$$

where  $I(x) = I_{max} f(x)$  is the total intensity distribution of the standing wave light field of period  $\lambda/2$ ,  $I_{max}$  is the maximum intensity, and  $f(x)$  describes the normalized modulation of the light field. For such a standing wave, the optical electric field (and the Rabi frequency) at the antinodes is double that of each travelling wave that composes it, and so the total intensity  $I_{max}$  at the antinodes is four times that of the

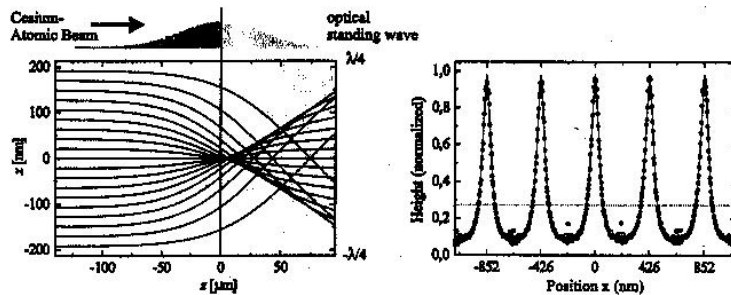
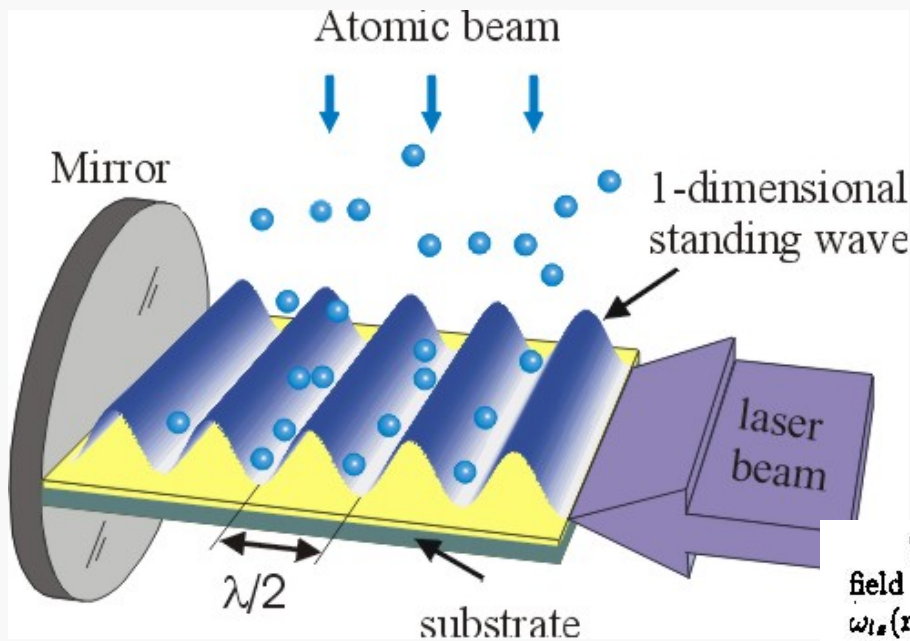
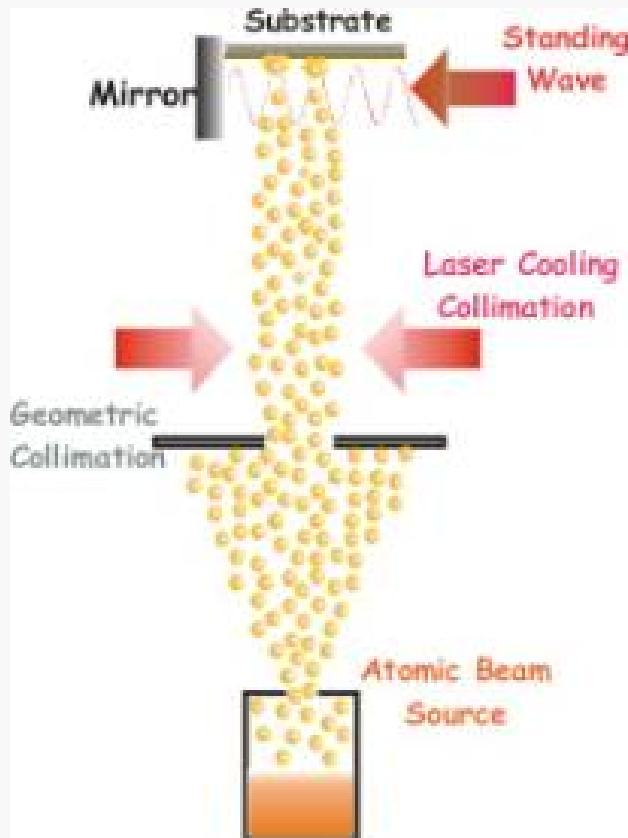


**Figure 3.** Left: Numerically calculated trajectories of a laser cooled beam of atoms focussed to the center of a Gaussian envelope standing wave light field (thick lens limit). The focussed laser beam forming the optical standing wave is clipped by the substrate. Note the different scales in x- and z-directions. Right: Analysis [25] of flux concentration for a realistic beam of thermal cesium atoms with 0.1 m/s transversal rms velocity at the focal plane  $z=0$ . The dotted line shows the flux distribution without the standing optical wave.

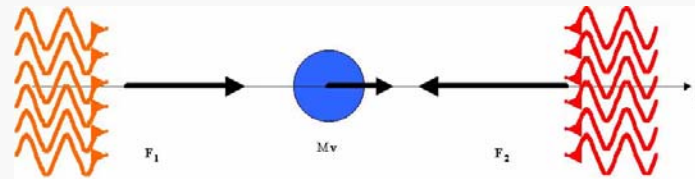
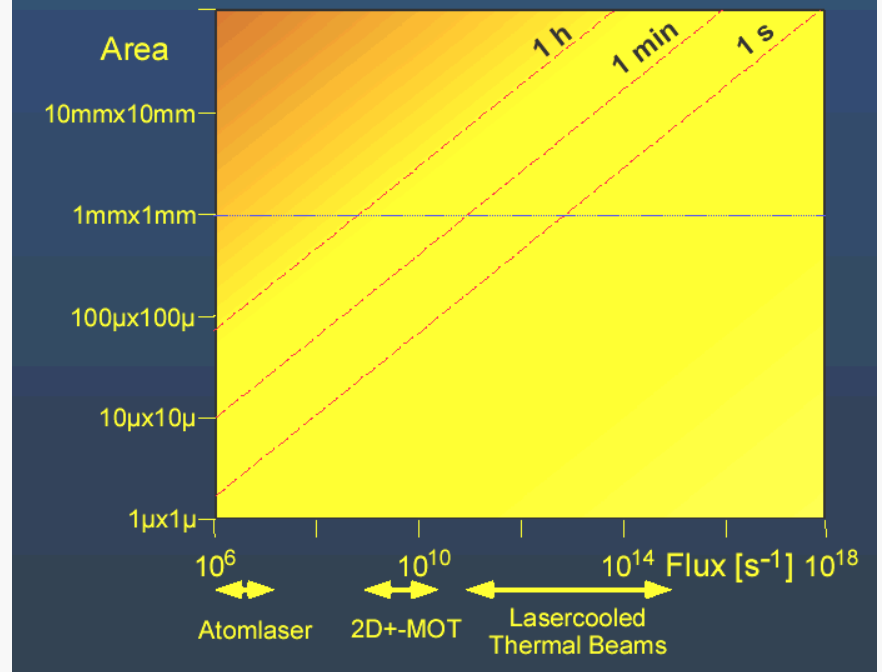
**The standing wave behaves like an array of microlenses for the atoms (in terms of atom optics)**

# Beams for atom lithography

1. **Intensity** --> reasonable exposure times
2. **Collimation** --> reduce aberration effects



## Which atom source for ANF?



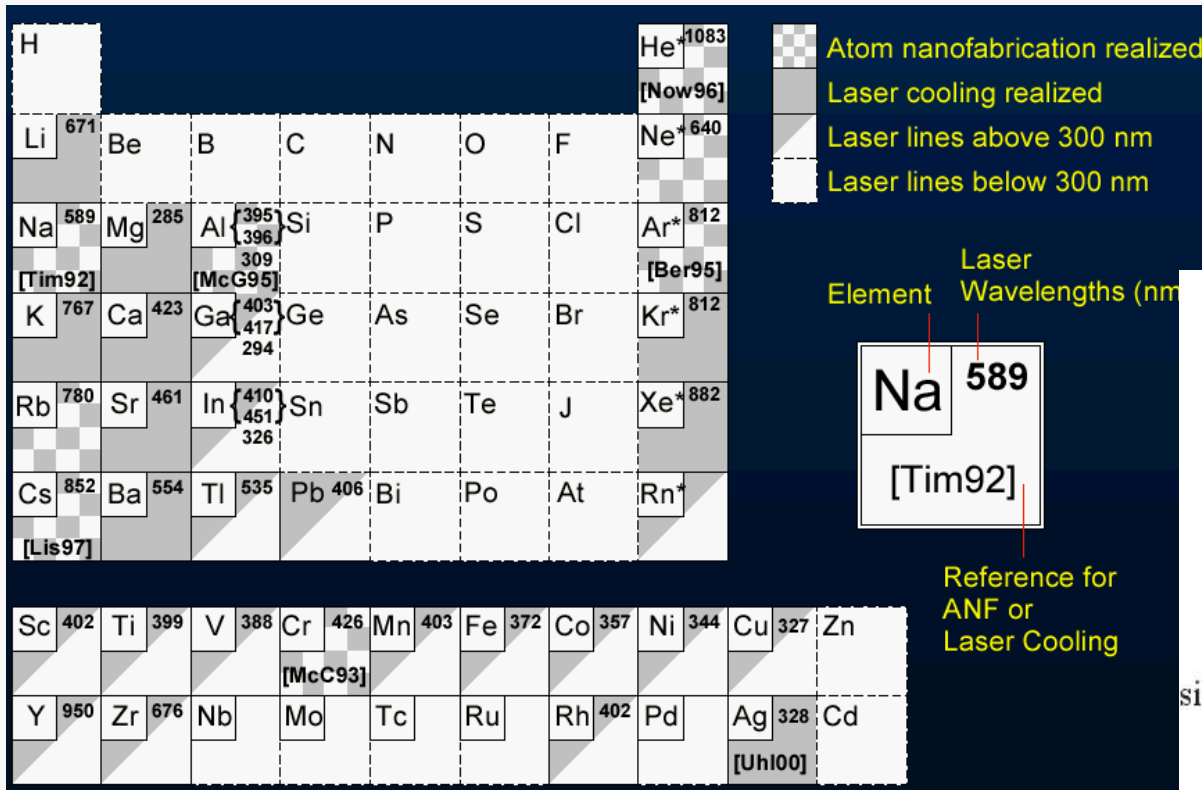
Optical molasses

$$F = F_1 - F_2 \approx 4v(\omega - \omega_{12})\hbar k^2 \langle n_{sp} \rangle \frac{1}{(\Gamma_s / 2)^2 + (\omega - \omega_{12})^2} \equiv -M\gamma v$$

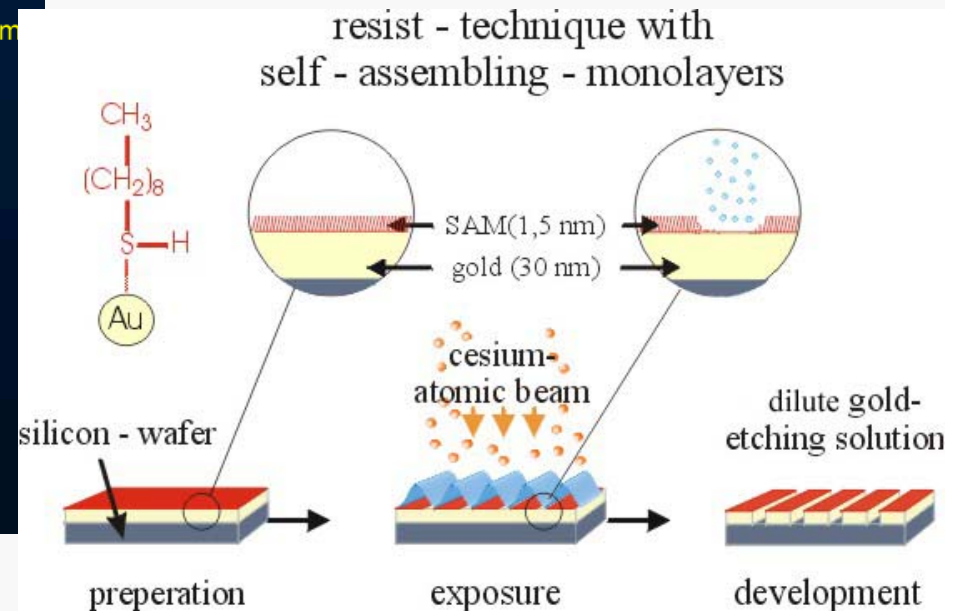
**Laser cooling technologies enable a suitable beam conditioning**

# Applicability of atom lithography

Atom species must be laser manipulated (wavelength, closed transitions,...)



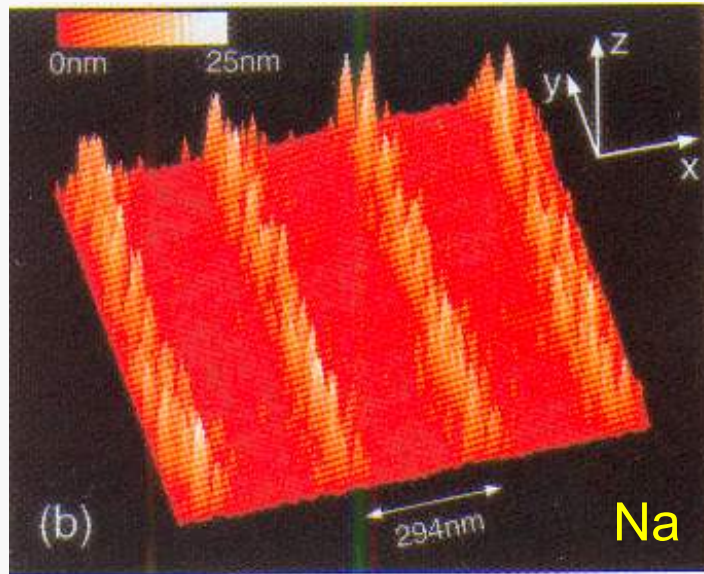
Materials to be employed in resist-assisted atom lithography  
alkanethiols self-assembling monolayers (SAM)



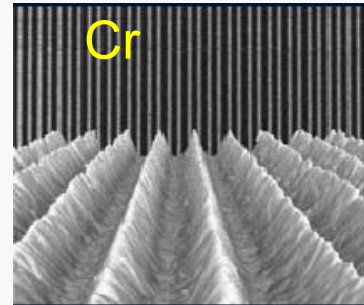
The technique can be applied only to a few atom species (at least, so far)

Atom	T <sub>S</sub> K	λ nm	γ 10 <sup>7</sup> /s	v <sub>c</sub> m/s	θ <sub>c</sub> mrad	5/ω <sub>r</sub> μs	2r <sub>c</sub> mm	P <sub>c</sub> mW	Θ <sub>D</sub> mrad	Θ <sub>R</sub> mrad	P <sub>ANF</sub> mW
<sup>4</sup> He*	300	1083	1.0	1.7	1.5	19	0.03	0.03	0.36	0.11	0.40
<sup>23</sup> Na	630	589	6.2	5.8	13	32	0.18	1.0	0.89	0.09	0.12
<sup>27</sup> Al	1640	309	8.2	4.0	4.0	10	0.04	6	0.44	0.07	0.95
<sup>40</sup> Ar*	300	812	3.6	4.8	17	105	0.49	0.5	0.68	0.05	0.15
<sup>52</sup> Cr	1825	426	3.1	2.1	3.5	37	0.08	2.4	0.26	0.03	2.0
<sup>56</sup> Fe	1920	372	1.6	1.0	1.3	31	0.03	1.5	0.18	0.04	4.6
<sup>70</sup> Ga	1555	403 417	4.9 9.2	3.1 6.1	5.2 10	45 48	0.14 0.29	4.3 7.8	0.35 0.48	0.03 0.03	1.1 0.59
<sup>108</sup> Ag	1435	328	1.4	7.2	15	46	0.33	18	0.61	0.03	0.46
<sup>115</sup> In	1355	410 451	5.8 10.2	3.8 7.3	8.5 16	77 93	0.29 0.68	6.0 9.5	0.40 0.54	0.03 0.02	0.83 0.43
<sup>133</sup> Cs	410	852	3.3	4.5	20	383	1.7	3.3	0.55	0.02	0.21
<sup>197</sup> Au	1800	268	16.7	7.1	19	57	0.40	32	0.59	0.04	0.60

# Gallery of examples

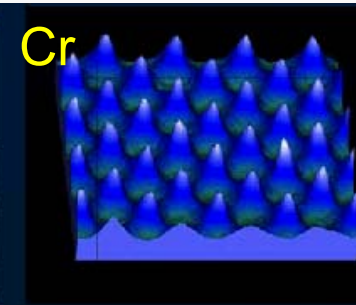


Timp et al. PRL 69 1636 (1992)



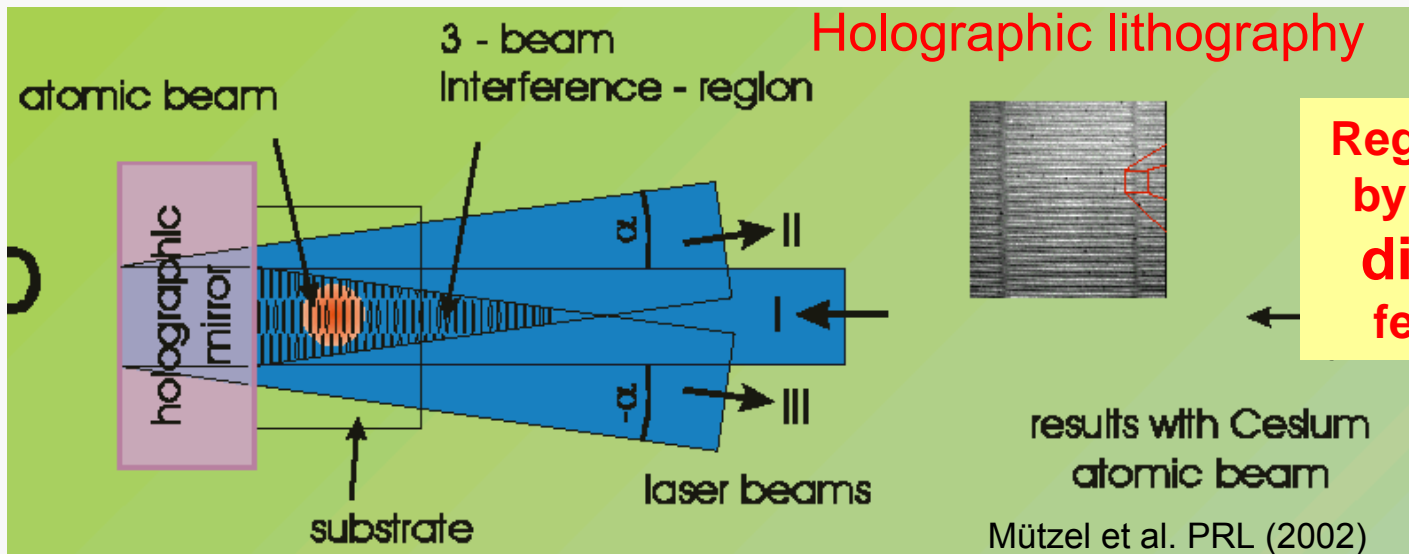
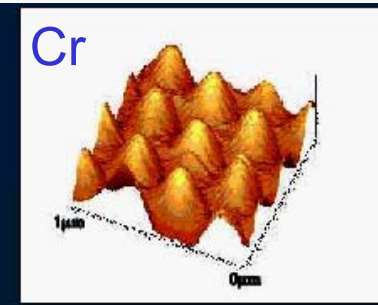
1D standing wave

McClelland et al.  
Science 87 262 (1993)



2D standing waves

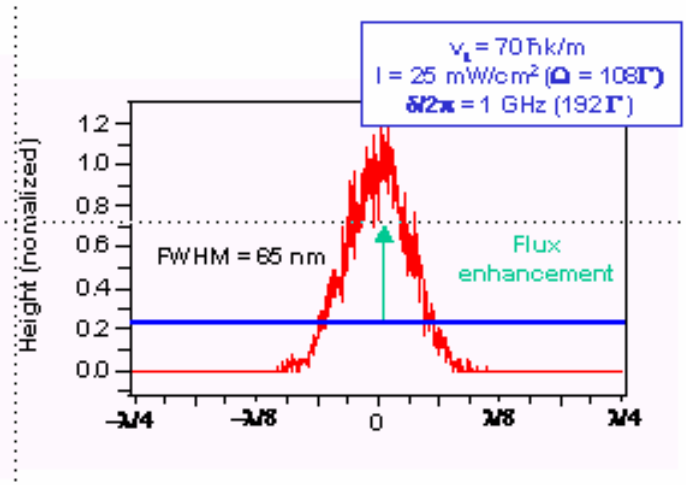
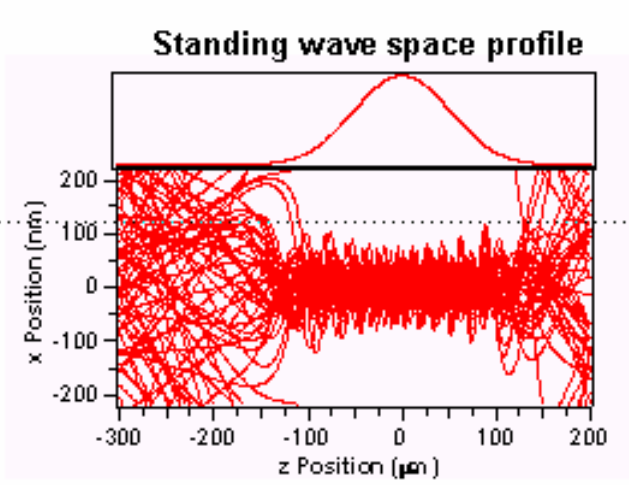
Gupta et al. APL 67 1378 (1995)  
Drozdofsky et al. Appl Phys B 65 755 (1997)



**Regular nanostructures built by either resist-assisted or direct deposition with feature size below 20 nm**

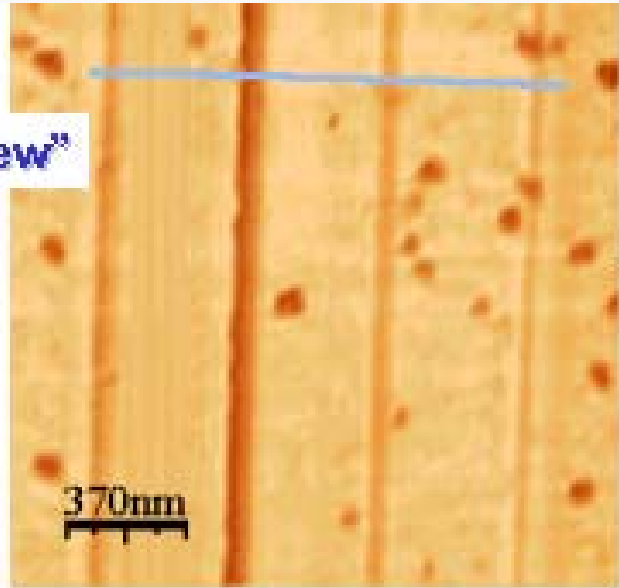
results with Cesium atomic beam  
Mützel et al. PRL (2002)

# Our "own" results (resist-assisted)



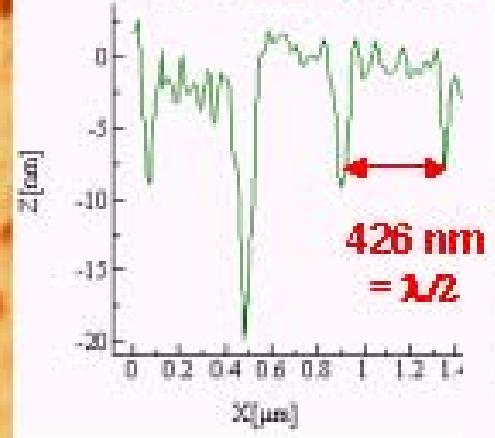
Due to the use of a "laser-cooled" atom beam (speed  $\sim 10 \text{ m/s}$ ), atoms are expected to be "channeled" instead of focused by the standing wave

"new"

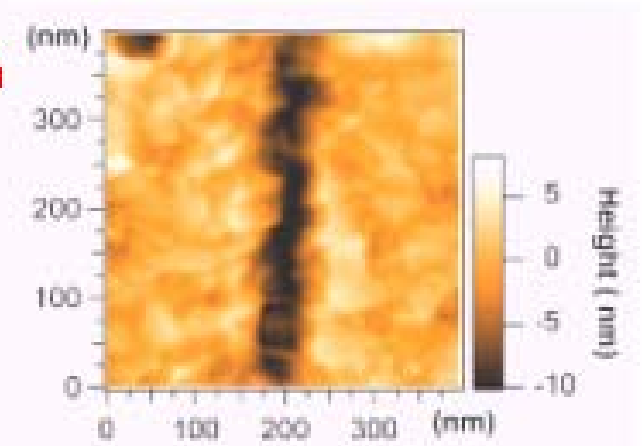


AFM image – plan view  
 Sputtered gold 30 nm thick  
 2h deposition and 13 min etching  
 Estimated dose: 2 atoms/SAM molecule

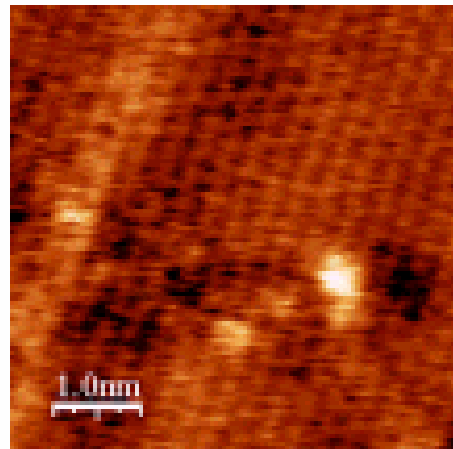
## AFM line profile



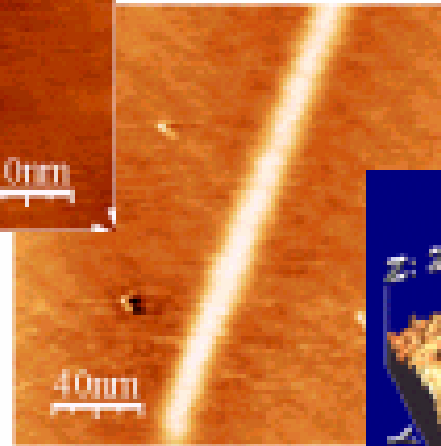
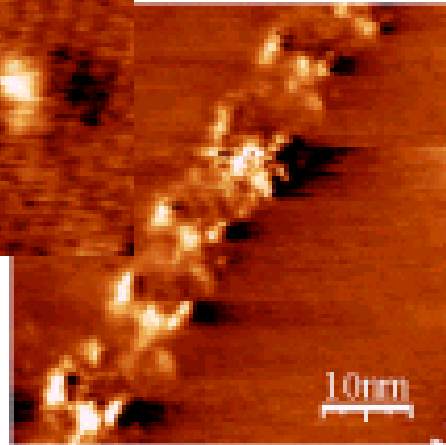
## Detail of a single trench



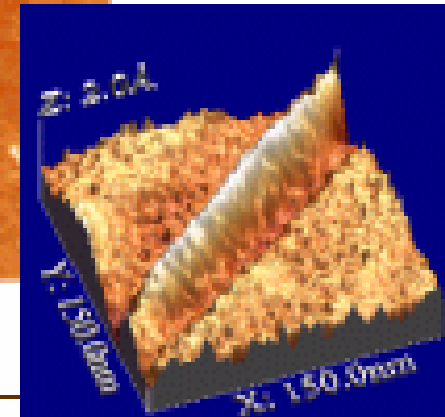
## Our “own” results (direct-deposition)



Structures with a variety of mo  
features observed after deposit  
optical mask



Assessment and  
interpretation still to be  
carried out



**Atom lithography (direct-deposition) may open the way  
for the *controlled* fabrication of nanostructures at the  
atom level (in a *bottoms-up* approach)**

# 7. An emerging simple nanotechnology: nanoimprint

## 9 Nanoimprint Lithography

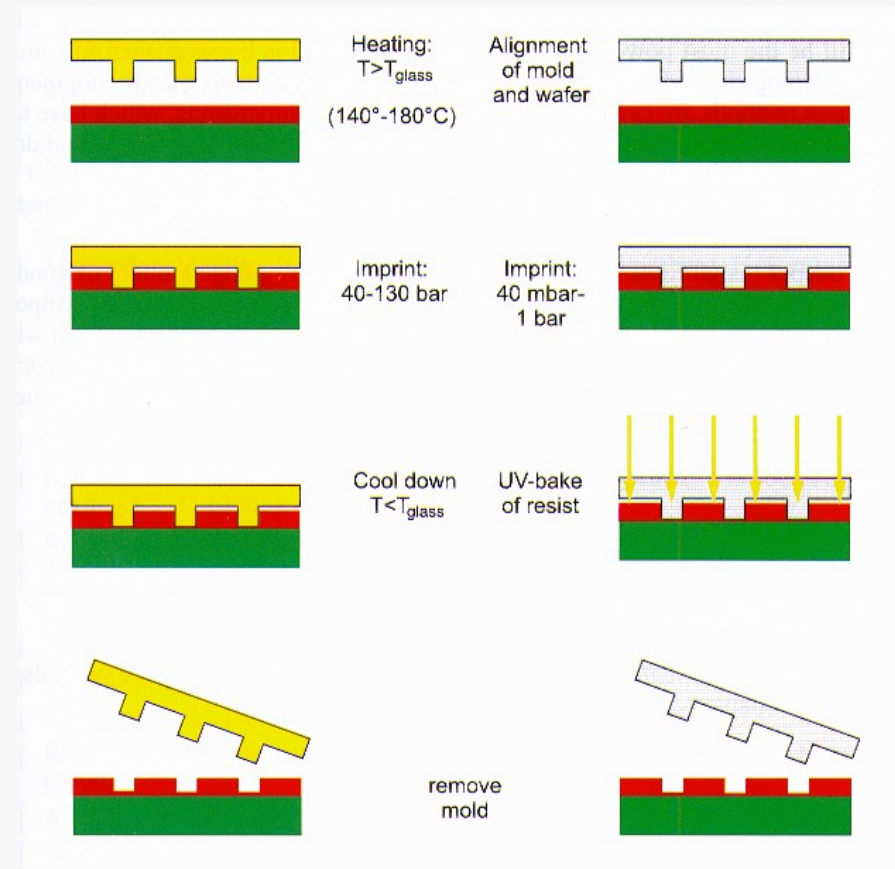
There are several approaches for patterning structures without lithographic methods, e.g. a silicon surface can be modified by depassivation by the tunneling current in a UHV-STM (Ultra High Vacuum Scanning Tunneling Microscope [20], [21], or the surface can be modified by the movement of an Atomic Force Microscope (AFM)-tip. A certain interest has been focused on the nanoimprint lithography (NIL), which is described in more detail in this section.

With the NIL a mold is processed by conventional technology, i.e. e-beam lithography and etching techniques, and is pressed onto a resist coated substrate. The structures in the mold are transferred into the resist and can be utilized after removing the mold. There are two different kinds of NIL, the hot embossing technique and a UV-based technique. A sketch of both techniques is given in Figure 29.

### Hot Embossing Technique

Here the sample is heated above the glass transition temperature of the resist, which is a thermoplastic polymer. Above that temperature the polymer behaves as a viscous liquid and can flow under pressure. The mold itself can be made of different materials, usually a silicon wafer with a thick  $\text{SiO}_2$  layer is used. This  $\text{SiO}_2$  layer is patterned and structured by e-beam lithography and anisotropic reactive ion etching. The aspect ratio of the features are 3:1 to 6:1, and the mold size is several  $\text{cm}^2$ . As thermoplastic polymers either PMMA (a well known e-beam resist) or novolak resin-based resists are in use. PMMA has a small thermal expansion coefficient of  $\sim 5 \times 10^{-5} \text{K}^{-1}$  and a small pressure shrinkage coefficient of  $\sim 3.8 \times 10^{-7} \text{psi}^{-1}$ . To ensure a proper removal of the mold, the resist is modified by release agents, which decrease the adhesion between mold and resist. Resist layers between 50 and 250 nm thickness are used. The imprint temperature and pressure are dependent on the resist. For PMMA the glass transition temperature is about  $105^\circ\text{C}$ , so the temperature at which the sample and the mold are heated is between  $140$  and  $180^\circ\text{C}$ . Then the mold is pressed onto the sample with pressures of about  $40 - 130 \text{ bar}$ . The temperature is then lowered below the glass transition temperature and the mold is removed. The features of the mold are now imprinted in the resist. The residual resist layer in these features is removed by anisotropic reactive ion etching.

Afterwards, the structures can be transferred to the substrate either by direct etching or by metal deposition and lift-off. Structures down to a feature size of  $10 \text{ nm}$  for holes and  $45 \text{ nm}$  for mesas are imprinted with a high accuracy [22]–[24].



**Soft-materials (e.g., organics) can be efficiently embossed at the nanoscale)**

# UV-assisted nanoimprint

## UV-based NIL

Heating and cooling of mold and sample is time-consuming. Therefore to achieve a somehow higher throughput, curing of the resist by UV irradiation is used. The thermoplastic resist is replaced by UV-curable monomers. The mold has to be fabricated of a UV-transparent material, e.g. quartz. The features are transferred to the mold by e-beam lithography and a Ti/PMMA resist stack. The patterned PMMA is used to transfer the features into the Ti, and the Ti is used to structure the quartz mold. The resists are acrylate- or epoxide-material systems, which can be modified with respect to low viscosity, UV curability, adhesion to the substrate and detachment from the mold. The low viscosity is essential for using low imprint pressures of 40 mbar – 1 bar. After pressing the mold on the sample, the sample is irradiated by UV-radiation through the mold and a baking, and hence a polymerization of the resist is initiated. This step lasts only about 90 seconds. After detaching the mold, the residual resist is removed by RIE and the further pattern transfer can be done. Again mold areas of several square centimeters can be imprinted in one run, and one imprint step takes about 10 minutes. The minimum feature size reported in the literature is 80 nm for dots. [25].

NIL offers the opportunity to define decananometer features in a rather simple manner, at least in comparison to the advanced lithography methods described above. The field size of  $\sim 2 \times 2 \text{ cm}^2$  is comparable to a die which is illuminated by a stepper. On the other hand, this method is time-consuming ( $>10 \text{ min}$  for one imprint) and up to now only structures on a plain surface have been investigated, while advanced lithography is able to define structures on textured substrates. Nevertheless, because of its technological simplicity, the NIL will be an alternative for research and small series production.

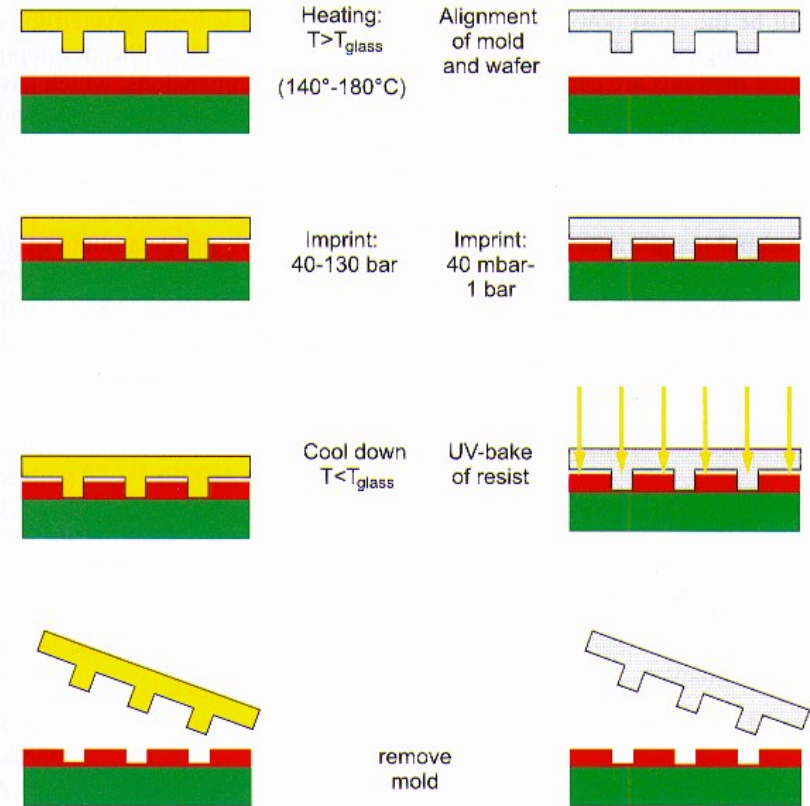


Figure 29: Nanoimprint lithography: hot embossing technique (left hand side) and UV nanoimprint (right hand side).

**Termomechanical or UV-assisted methods can be employed to replicate a master pattern with nanosized features (but how to make the original mask?)**

# Conclusions

- ✓ Optical lithography has been the dominant technique in microelectronics
- ✓ Fundamental limitations exist preventing its exploitation in the nanotechnology realm
- ✓ Efforts are being devoted to overcome limitations, but new approaches are (or will be soon) needed
- ✓ Electron microscopy and lithography allow for neglecting diffraction effects, but exhibit practical limitations as well
- ✓ Atom lithography might represent a viable alternative (also in view of bottoms-up implementations)
- ✓ Very simple and efficient methods, as nanoimprint, are emerging as well